

# Geophysical-Geochemical Modeling of Deep Crustal Compositions: Examples of Continental Crust in Typical Tectonic Settings and North China Craton

Dan-Dan Cui<sup>1</sup>, Jingliang Guo<sup>1</sup>, William Joseph Shinevar<sup>2</sup>, Liang Guo<sup>1</sup>, Wang Chun Xu<sup>1</sup>, Hongfei Zhang<sup>1</sup>, and Zhenmin Jin<sup>1</sup>

<sup>1</sup>China University of Geosciences (Wuhan)

<sup>2</sup>University of Colorado, Boulder

November 23, 2022

## Abstract

The chemical composition of the deep continental crust is key to understanding the formation and evolution of the continental crust. However, constraining the chemical composition of deep continental crust is limited by indirect accessibility. Here we present a modeling method to constrain deep crustal chemical structures from observed crustal seismic structures. We first compile a set of published composition models for the continental crust. Phase equilibria and compressional wave speeds (VP) are calculated for each composition model at a range of pressure and temperature (278–2223 MPa, 50–1200°C). Functional relationships are obtained between calculated wave speeds and crustal compositions at pressure and temperature conditions within the alpha( $\alpha$ )-quartz stability field. These relationships can invert observed seismic wave speeds of the deep crust to chemical compositions in regions with given geotherms (MATLAB code is provided). We apply these relationships to wave speed constraints of typical tectonic settings of the global continental crust and the North China Craton. Our method predicts that the lower crust in regions with thin- (e.g., rifted margins, rifts, extensional settings, and forearcs) or thick-crust (e.g., contractional orogens) is more mafic than previously estimated. The difference is largest in extensional settings ( $52.47 \pm 1.18$  and  $51.11 \pm 1.61$  vs. 59.37 wt. % SiO<sub>2</sub>). The obtained 2-D chemical structure of the North China Craton further shows features consistent with the regional tectonic evolution history and xenoliths. The obtained chemical structure can serve as a reference model from which chemical features in the deep crust can be recognized.

## Hosted file

2 supporting information.docx available at <https://authorea.com/users/543902/articles/601439-geophysical-geochemical-modeling-of-deep-crustal-compositions-examples-of-continental-crust-in-typical-tectonic-settings-and-north-china-craton>

## Hosted file

essoar.10512339.1.docx available at <https://authorea.com/users/543902/articles/601439-geophysical-geochemical-modeling-of-deep-crustal-compositions-examples-of-continental-crust-in-typical-tectonic-settings-and-north-china-craton>

Dan-Dan Cui<sup>1</sup>, Jing-Liang Guo<sup>1, \*</sup>, William J. Shinevar<sup>2</sup>, Liang Guo<sup>1</sup>, Wang-Chun Xu<sup>1</sup>, Hong-Fei Zhang<sup>1</sup>, Zhen-Min Jin<sup>1</sup>

<sup>1</sup>State Key Laboratory of Geological Processes and Mineral Resources, School of Earth Sciences, China University of Geosciences, Wuhan 430074, China

<sup>2</sup>Department of Geological Sciences, University of Colorado Boulder, Boulder, CO 80309, USA

Corresponding author: \*Jing-Liang Guo (jl.guo@cug.edu.cn)

Key Points:

- We present a geophysical-geochemical modeling method to derive a chemical structure of deep continental crust from its  $V_p$  structure.
- We apply this method to various tectonic settings of the global lower continental crust and the North China Craton.
- The inferred chemical structure serves as a reference model from which crustal heterogeneity can be highlighted.

Abstract

The chemical composition of the deep continental crust is key to understanding the formation and evolution of the continental crust. However, constraining the chemical composition of deep continental crust is limited by indirect accessibility. Here we present a modeling method to constrain deep crustal chemical structures from observed crustal seismic structures. We first compile a set of published composition models for the continental crust. Phase equilibria and compressional wave speeds ( $V_p$ ) are calculated for each composition model at a range of pressure and temperature (278–2223 MPa, 50–1200°C). Functional relationships are obtained between calculated wave speeds and crustal compositions at pressure and temperature conditions within the alpha( )-quartz stability field. These relationships can invert observed seismic wave speeds of the deep crust to chemical compositions in regions with given geotherms (MATLAB code is provided). We apply these relationships to wave speed constraints of typical tectonic settings of the global continental crust and the North China Craton. Our method predicts that the lower crust in regions with thin- (e.g., rifted margins, rifts, extensional settings, and forearcs) or thick-crust (e.g., contractional orogens) is more mafic than previously estimated. The difference is largest in extensional settings ( $52.47 \pm 1.18$  and  $51.11 \pm 1.61$  vs.  $59.37$  wt. %  $\text{SiO}_2$ ). The obtained 2-D chemical structure of the North China Craton further shows features consistent with the regional tectonic evolution history and xenoliths. The obtained chemical structure can serve as a reference model from which chemical features in the deep crust can be recognized.

### Plain Language Summary

The chemical composition of the deep continental crust is critical for understanding the formation and evolution of the continental crust. However, due to lim-

ited accessibility, the composition of the deep crust is difficult to constrain. The seismic wave speed of the crust can be used to derive its chemical composition because wave speed is strongly dependent on the mineral assemblage, and mineral assemblage is strongly dependent on bulk chemical composition. Here we present a geophysical-geochemical modeling method to construct chemical structures from compressional wave speed structures of deep continental crust. This method is based on functional relationships between published model crustal compositions and their corresponding wave speeds calculated for different pressure and temperature conditions. We apply this method to type sections of the global continental crust and the North China Craton. The results suggest that (1) current lower crustal composition models for regions with thin or thick crust may need reevaluation, and (2) spatial chemical compositions in the deep crust can be linked to the history of regional tectonic evolution.

## 1 Introduction

The deep continental crust (refers to as the combination of middle crust and lower crust) is the main place where crustal growth, reworking, recycling, and relamination occur Arndt & Goldstein, 1989; Hacker et al., 2015; Jagoutz & Behn, 2013; Rudnick & Gao, 2003; Willbold & Stracke, 2010(;; ;). Crustal growth by basaltic underplating produces juvenile mafic lower crust Arndt & Goldstein, 1989(). Crustal reworking through intra-crustal partial melting, crystal fractionation, and mixing processes facilitates intra-crustal differentiation Rudnick & Gao, 2003(). Recycling of dense lower crustal materials into the mantle, or relamination of buoyant felsic materials from subducting slabs to the lower crust, drives the lower and the bulk continental crust to more felsic compositions Hacker et al., 2015; Jagoutz & Behn, 2013; Willbold & Stracke, 2010(;; ;). The composition of the deep crust also influences the rheology, surface elevation, and regional mineralization of the continental crust e.g., Hou et al., 2017; Jiménez-Munt et al., 2008; Lee et al., 2012; Shinevar et al., 2015(;; ;). Despite its importance, the composition of the deep continental crust is still in dispute. Rudnick and Fountain (1995) and Rudnick and Gao (2003, 2014) estimated the average lower crustal composition to be mafic ( $\text{SiO}_2$  53 wt. %) based on wave speeds of the lower crust and compositions of lower-crustal xenoliths. Conversely, Hacker et al. (2015) argue that the lower crust could be andesitic in composition (potential  $\text{SiO}_2$  varying from 49–62 wt. %) based on heat flow, wave speeds, and representative rock compositions.

Estimating the deep crustal composition is difficult due to limited accessibility and petrological heterogeneity in the deep crust Taylor & McLennan, 1985; Thybo & Artemieva, 2013(;). Exhumed high-grade metamorphic terrains or xenoliths entrained to the surface by magmatic rocks can provide direct constraints on the deep crustal composition Gao et al., 1998a; Guo et al., 2020; Liu et al., 2001; Rudnick & Taylor, 1987; Shaw et al., 1994; Weaver & Tarney, 1984(;; ;). However, the occurrence of deep crustal samples is overall limited (Rudnick and Gao, 2003,

2014). Crustal compositions can also be inferred from crustal seismic properties, since the crustal composition has a fundamental control on the mineral assemblage and therefore the wave speed of deep crust Behn & Kelemen, 2003Christensen & Mooney, 1995Hacker et al., 2015Rudnick & Fountain, 1995Zhang et al., 2008(;; ;). Geophysical explorations have provided wave speed profiles of the crust in numerous regions worldwide Mooney, 2015(), offering the basis for deriving large-scale chemical compositional information on the present-day continental crust Artemieva & Shulgin, 2019().

Before deriving chemical information from crustal seismic wave speeds, one needs to determine the relationship between wave speed and rock composition (e.g.,  $\text{SiO}_2$ ). One common approach is to use natural samples with known chemical compositions. The wave speeds of natural rocks can be measured and then extrapolated to different pressure and temperature (P-T) conditions, assuming a linear dependence of wave speeds on P-T above the confining pressure Christensen & Mooney, 1995Kern & Schenk, 1985(e.g., 600MPa in ;). These wave speeds can be compared with seismic observations to estimate composition. A problem with this methodology is that the mineralogy of a rock changes with P-T conditions, which results in a nonlinear dependence of seismic wave speed on P-T conditions Diaferia & Cammarano, 2017Zertani et al., 2019(;). Hence, the linearly extrapolated wave speeds might suffer potential disequilibrium issue. Alternatively, the wave speeds of natural rocks can be calculated by integrating thermodynamically calculated or observed modal mineralogy with mineral physical properties Abers & Hacker, 2016Behn & Kelemen, 2006Gao et al., 2000Hacker et al., 2015Sammon et al., 2020Sammon et al., 2022(e.g., ; ; ; ;). However, wave speed does not uniquely map to oxide composition. For example, granulite-facies rocks ranging in composition from 50–66 wt. %  $\text{SiO}_2$  can have the same calculated compressional wave speed ( $V_P$ ) Figure 9 in Hacker et al., 2015(). The nonuniqueness of deep crustal lithologies leads to uncertainties in estimated crustal composition Behn & Kelemen, 2003Hacker et al., 2015(;). Therefore, a common practice is to select the composition- $V_P$  relationships of two or three ‘typical’ deep crustal lithologies to estimate the crustal composition Christensen, 1996Christensen & Mooney, 1995Rudnick & Fountain, 1995Zhang et al., 2008(;; ;). Since the pioneering work of Clarke (1889), numerous studies have provided estimates of crustal compositions at global or regional scales Gao et al., 1998aLiu et al., 2001Rudnick & Gao, 2003Taylor & McLennan, 1985Wedepohl, 1995(e.g., ; ; ; ;). Unlike natural rocks that span widely in chemical composition and wave speed, model compositions of the continental crust show overall consistent variation patterns that can be utilized to calculate wave speed-composition correlations (Section 2 below).

In this study, we present a geophysical-geochemical modeling method of calculating crustal compositions from observed  $V_P$  of the deep crust based on compiled crustal composition models. Combining crustal model compositions with thermodynamic phase calculations avoids assignment of deep crustal lithologies as well as the potential disequilibrium issue regarding measured  $V_P$  of these lithologies. We apply this method to type sections of the continental crust

and the North China Craton (NCC) to estimate the deep crustal compositions. The results show that the lower crust in cratons and orogens has intermediate compositions, while the lower crust in subduction- and rifting-related regions have mafic compositions. We utilize the obtained compositional structure of a specific region to infer the regional tectonic evolution history.

## 2 Methods

### 2.1 Model Crustal Compositions

We compiled 172 published chemical models of the crust, which were mostly estimated for the continental crust (Table S1). The chemical models include those for the bulk or specific parts of the global continental crust Hacker et al., 2015; Rudnick & Gao, 2003; Shaw et al., 1994 (e.g., ; ; ), continental arcs e.g., Ducea et al., 2015(), intra-oceanic arcs e.g., Jagoutz & Kelemen, 2015(), cratons, orogenic belts, extensional regions in China Gao et al., 1998a(), and oceanic crust e.g., White & Klein, 2014() (Figure 1h). The model compositions vary from mafic in the lowermost part of thickened arc crust to granitic in the upper continental crust Rudnick & Gao, 2003; Taylor & McLennan, 1985 (e.g., ; ), covering the possible chemical variability in the deep continental crust ( $\text{SiO}_2$  from 47.90–70.70 wt. %).

Oxides that have large variations, including  $\text{CaO}$ ,  $\text{MgO}$ ,  $\text{FeO}_T$ , and  $\text{K}_2\text{O}$ , show good linear correlations with  $\text{SiO}_2$  ( $R^2 > 0.6$ ; Figure 1a-d, where  $R^2$  is the coefficient of determination for linear regression.). The variations in  $\text{Al}_2\text{O}_3$ ,  $\text{TiO}_2$ , and  $\text{Na}_2\text{O}$  are relatively small, and their correlations with  $\text{SiO}_2$  are thus poor ( $R^2 < 0.6$ ) (Figures 1e-g).

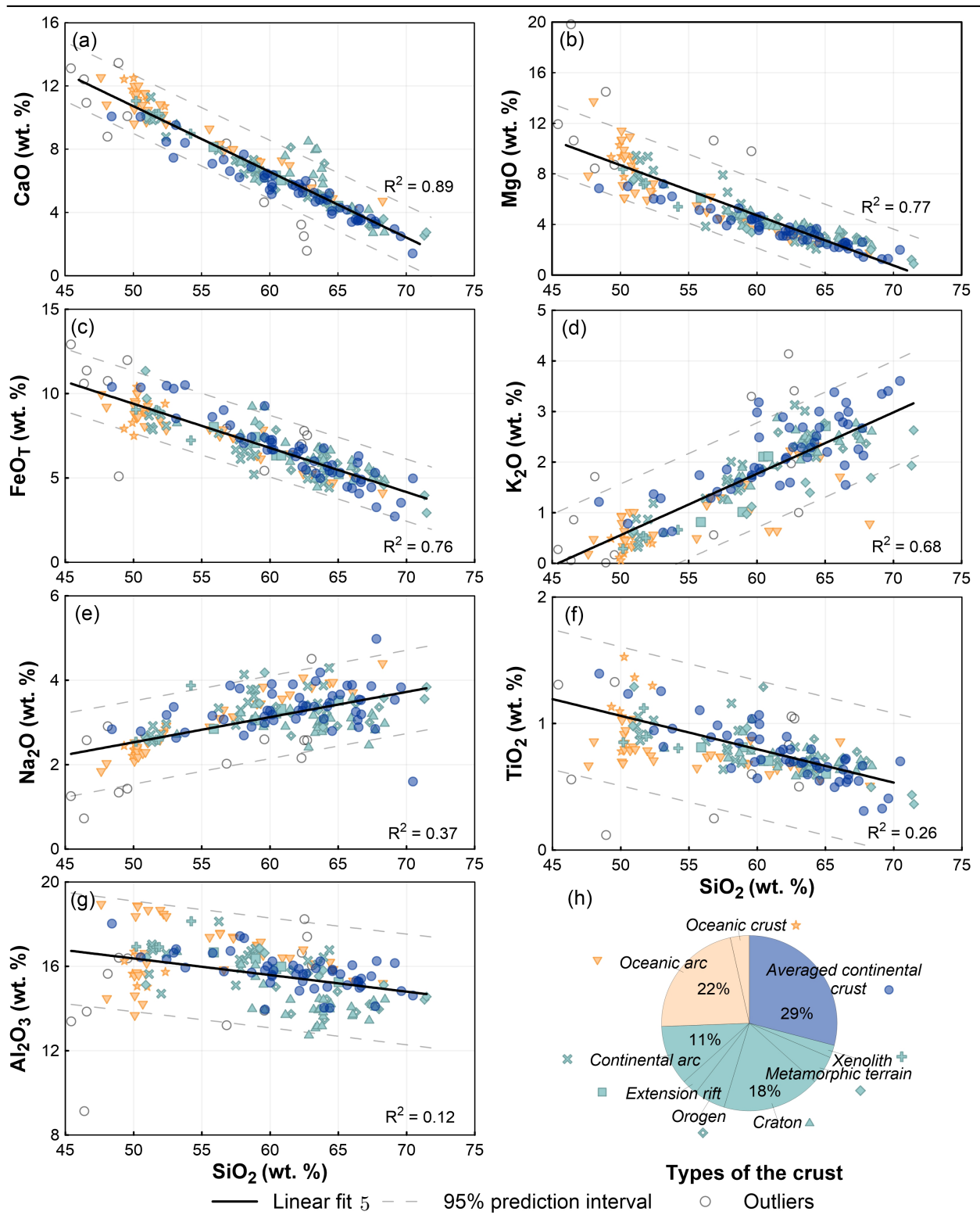
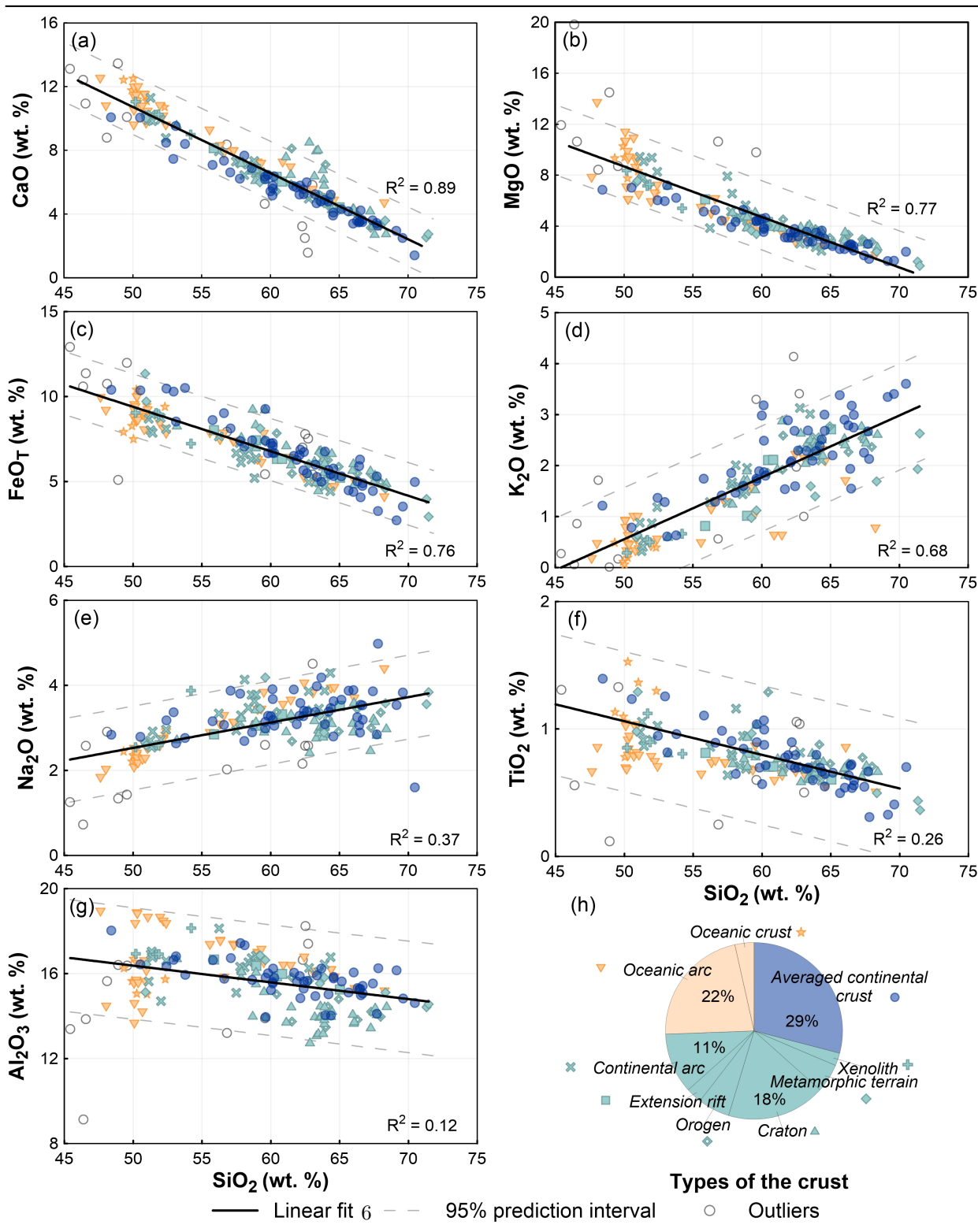


Figure 1. Correlations between major oxides of published crustal model compositions. (a-g) Covariation between



## 2.2 Calculating Wave Speeds for Model Crustal Compositions

We use thermodynamic calculation software `Perple_X` (ver. 6.9.1, downloaded on October 25, 2021) Connolly, 2009(), a Gibbs free energy minimization program, to calculate wave speeds for the compiled model crustal compositions. We first calculated phase equilibria for all crustal compositions at broad P-T ranges. The considered depths range from 10 to 80 km (278–2223 MPa) in an interval of 1 km, and the temperature ranges are 50–700°C at 10–15 km (278–417 MPa), 100–900°C at 16–35 km (445–973 MPa), 300–1000°C at 36–55 km (1000–1528 MPa), 400–1200°C at 56–80 km (1556–2223 MPa). The corresponding pressure ( $P$ ) at depth was calculated from  $P = gz$ , where  $\rho$  is the average density of the continental crust (2.835 g/cm<sup>3</sup>, Christensen & Mooney, 1995),  $g$  is the gravitational acceleration (9.8 m/s<sup>2</sup>), and  $z$  is the depth in km. A threshold temperature, the temperature at which subsolidus metamorphic reactions are stopped in our calculations, of 500°C is a reasonable lower bound for net transfer reactions under hydrous crustal conditions, and a new equilibrium is considered unreachable at temperatures < 500°C Austrheim, 1998(). Thus an equilibrium threshold temperature of 500°C was used for calculating phase equilibria following previous studies Guo et al., 2020 Shinevar et al., 2018(; ).

Thermodynamic dataset `ds62` from Holland and Powell (2011) and mineral solution models in Green et al. (2016) were used in the calculation (Table S2). Ten major components (Na<sub>2</sub>O–CaO–K<sub>2</sub>O–FeO–MgO–Al<sub>2</sub>O<sub>3</sub>–SiO<sub>2</sub>–H<sub>2</sub>O–TiO<sub>2</sub>–Fe<sub>2</sub>O<sub>3</sub>, NCKFMASHTO) were considered. Most of the reported crustal composition models bear no water and Fe<sup>3+</sup> data. The presence of water may significantly change the physical property of the crust Guerri et al., 2015(). Hacker et al. (2015) assumed 0.5 wt. % and 1 wt. % H<sub>2</sub>O contents for amphibolite-facies and granulite-facies xenoliths and terrains, typical metamorphic rocks in the deep crust. We conducted two sets of calculations assuming 0.5 and 0.75 wt. % H<sub>2</sub>O in the deep crust. The ratio of Fe<sup>3+</sup> to total Fe, which is expressed as Fe<sup>3+</sup>/Fe, is related to the oxygen fugacity of the system. Ratios of Fe<sup>3+</sup>/Fe in global arc basaltic melt inclusions are 0.18 to 0.32 Kelley & Cottrell, 2009(). The choice of Fe<sup>3+</sup>/Fe in this range for phase equilibrium and wave speed calculations induces only a small variation in calculated  $V_P$  (mostly within  $\pm 0.04$  km/s) (Figure S1), suggesting that the calculated  $V_P$  is insensitive to Fe<sup>3+</sup>/Fe. Thus, we chose Fe<sup>3+</sup>/Fe = 0.25 for all calculations.

Wave speeds were calculated in `Perple_X` by implementing elastic moduli, mineral density, and phase transition data between alpha-beta (-) quartz Abers & Hacker, 2016 Jagoutz & Behn, 2013(; ). The elastic moduli of minerals, including bulk modulus (K) and shear modulus ( $\mu$ ), have been reported for most major crustal minerals. For minerals whose elastic moduli are not provided in `Perple_X`, their K values were derived from the Gibbs free energy, and  $\mu$  values were computed from K and the average Poisson’s ratio (0.265) for the continental crust Christensen, 1996(). The Voigt-Reuss-Hill averaging method was used to calculate the elastic moduli of a given mineral assemblage, from which

seismic wave speeds were further derived Connolly & Kerrick, 2002(). For equilibrium phases with melts, only solid phases (excluding the liquid phase) were considered to calculate  $V_P$  and bulk chemical compositions.

### 2.3 Establishing Functional Relationships Between $V_P$ and Oxide Contents

Functional relationships were established between  $V_P$  and oxide contents of crustal composition models for each P-T condition by using the regress function in MATLAB. Second-order polynomial fitting was used, because it yielded slightly higher  $R^2$  and smaller root mean square error (RMSE) than that of linear fitting, but similar to the values yielded with cubic fitting. Taking the result of the second-order polynomial fitting at the P-T condition of 30 km (833 MPa) and 500°C as an example,  $V_P$  shows strong negative correlations with  $\text{SiO}_2$  ( $R^2 = 0.98$ ) and  $\text{K}_2\text{O}$  ( $R^2 = 0.74$ ), positive correlations with  $\text{CaO}$  ( $R^2 = 0.93$ ),  $\text{MgO}$  ( $R^2 = 0.91$ ), and  $\text{FeO}_T$  ( $R^2 = 0.79$ ), and weaker correlations with  $\text{Na}_2\text{O}$  ( $R^2 = 0.48$ ),  $\text{TiO}_2$  ( $R^2 = 0.44$ ), and  $\text{Al}_2\text{O}_3$  ( $R^2 = 0.24$ ) (Figure 2). The RMSEs for the fitted functions of  $V_P$  with  $\text{SiO}_2$ ,  $\text{K}_2\text{O}$ ,  $\text{CaO}$ ,  $\text{MgO}$ , and  $\text{FeO}_T$  are 0.77, 0.45, 0.69, 0.71, and 0.80 wt. %, respectively (Figure 2).

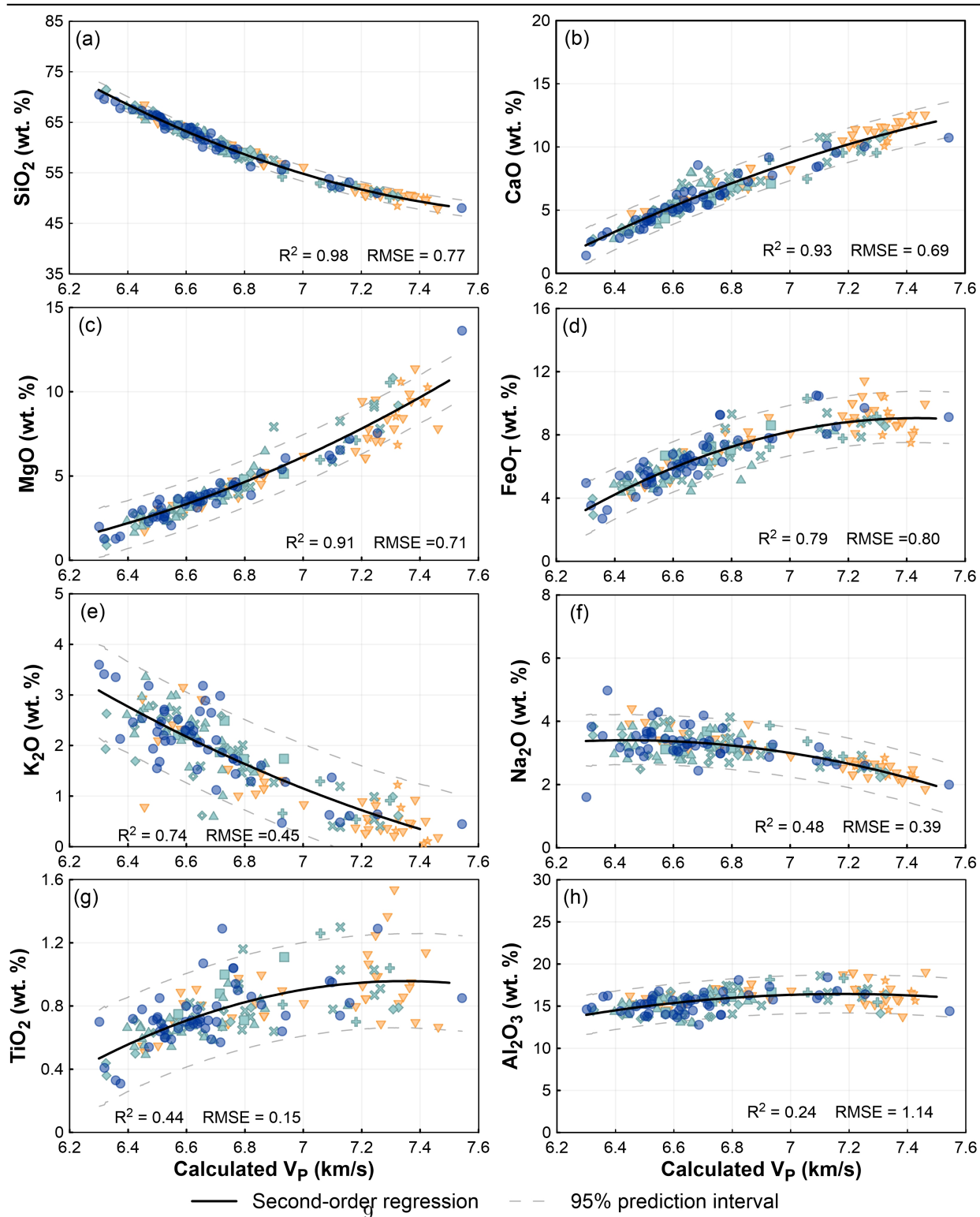
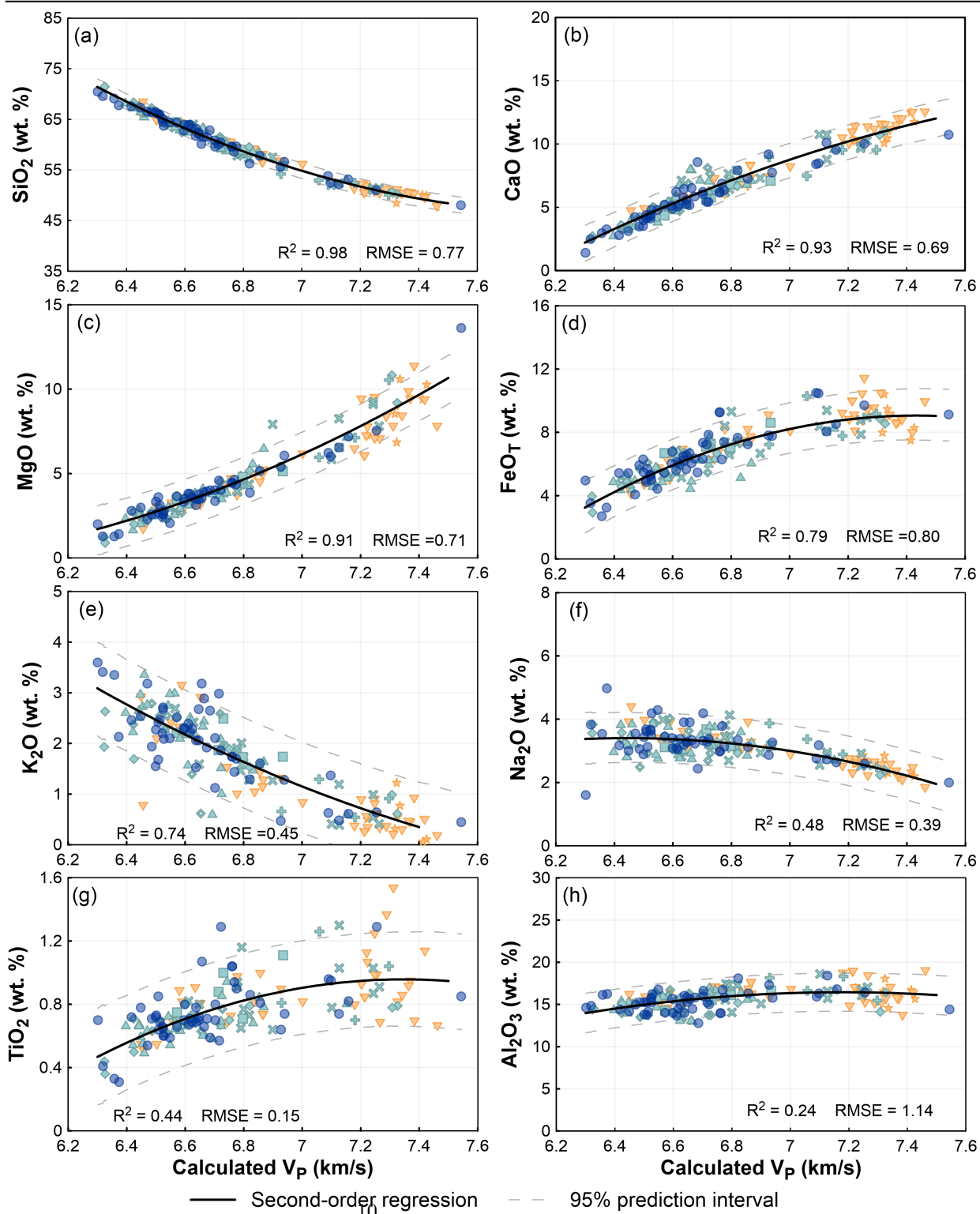
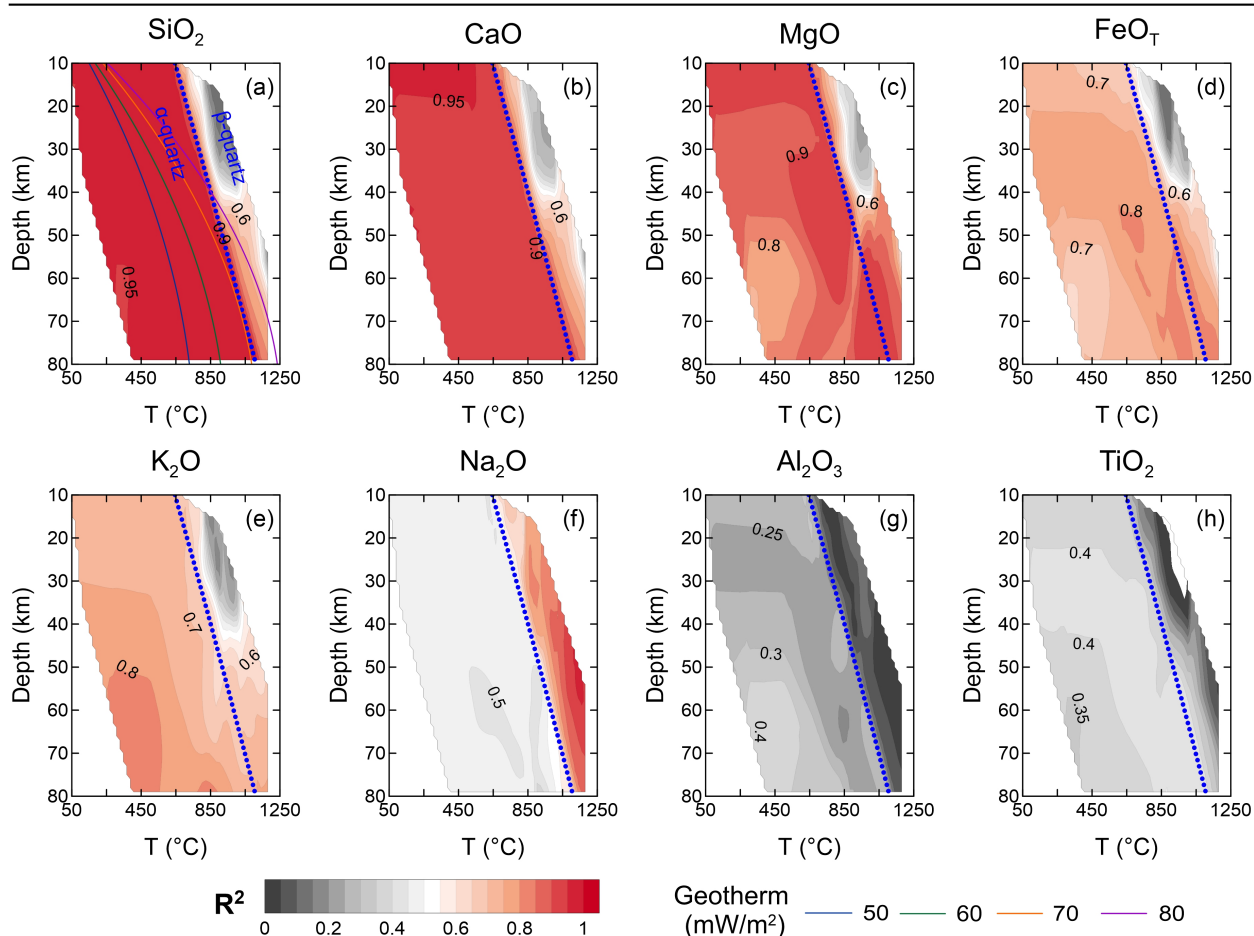


Figure 2. Relationships between calculated  $V_p$  and major oxides of crustal composition models at 30 km and



The correlations are strong ( $R^2 > 0.7$ ) between  $V_P$  with  $\text{SiO}_2$ ,  $\text{CaO}$ ,  $\text{MgO}$ ,  $\text{FeO}_T$ , and  $\text{K}_2\text{O}$  in the stability field of  $\alpha$ -quartz (Figure 3). At higher temperatures in the  $\alpha$ -quartz stability field,  $V_P$  becomes less correlated with all oxide contents (Figure 3). Given that  $\alpha$ -quartz has a higher  $V_P$  than  $\beta$ -quartz at the same condition Abers & Hacker, 2016(), the  $\alpha$ -quartz phase transition increases the calculated  $V_P$  of felsic compositions which contain quartz but less for those of more mafic compositions which contain little or no quartz. The phase transition of  $\alpha$ -quartz thus perturbs the correlation between  $V_P$  and the oxide contents (Figure S2). However, this transition is not expected in the crust with normal geothermal gradients (e.g., surface heat flow values of  $< 70 \text{ mW/m}^2$ ), but the transition is expected in the hot crust with surface heat flow values of 70 and  $80 \text{ mW/m}^2$  at depths  $> 70$  and  $> 40 \text{ km}$ , respectively (Figure 3; Chapman,1986).



**Figure 3.** The robustness of  $V_P$ -composition regression at crustal P-T conditions.  $R^2$  is the coefficient of det

## 2.4 Inverting Crustal Compositions from Observed Crustal $V_P$ for a Specific Region

To calculate crustal compositions from observed  $V_P$  in the deep crust of a specific region, one should first assign local geotherms. Geotherms can be calculated from mean surface heat flow values, assuming a steady-state transfer of conductive heat Chapman, 1986():

$$T(z) = T_0 + \frac{q_0}{k}z - \frac{Az^2}{2k} \quad (1)$$

where  $T_0$  is surface temperature ( $^{\circ}\text{C}$ ),  $q_0$  is surface heat flow ( $\text{mW}/\text{m}^2$ ),  $k$  is thermal conductivity ( $\text{W}/\text{m}/\text{K}$ ), and  $A$  is volumetric heat production ( $\text{W}/\text{m}^3$ ), and  $z$  is depth ( $\text{km}$ ).  $T_0$  was set to  $10^{\circ}\text{C}$  at the surface. Thermal parameters  $k$  and  $A$  are generally assumed as constants for each crustal layer that was defined from the seismic structure of the crust Chapman, 1986(). The values of  $k$  and  $A$  are controlled by crustal compositions and can be estimated from local samples (see Section 3.2.2 for example).

We provide a MATLAB-based user-friendly graphical user interface (GUI) for the inverting process (CalcCrustComp). With given depth and temperature, users can invert deep crustal composition (major elements oxide) from crustal  $V_P$  using the  $V_P$ -composition functional relationships established for model crustal compositions.

## 2.5 Uncertainty Analysis

Uncertainties in the inverted crustal compositions have four major sources: (1) observed crustal  $V_P$ , (2) local geotherms, (3) assumed water contents in the crust, and (4) established  $V_P$ -composition relationships.

1. The uncertainty in crustal  $V_P$  obtained from wide-angle reflection or refraction experiments is typically  $\pm 0.2 \text{ km/s}$  Zhang et al., 2013(). An uncertainty of  $0.1 \text{ km/s}$  in  $V_P$  would result in an uncertainty of  $\sim 2.5 \text{ wt. \%}$  in the calculated  $\text{SiO}_2$  content of the crust (Figure 2a), which is larger than the RMSE (average  $1 \text{ wt. \%}$ ) of  $V_P$ - $\text{SiO}_2$  regression.
2. The uncertainty in local geotherm largely depends on the uncertainty in measured surface heat flow Chapman, 1986(). A  $10\%$  uncertainty ( $6$  for  $60 \text{ mW}/\text{m}^2$ ) in the measured surface heat flow results in a  $10\text{--}15\%$  ( $60\text{--}90$  for  $600^{\circ}\text{C}$ ) uncertainty for Moho temperature Chapman, 1986Liu et al., 2016(; ). Higher temperatures result in lower  $V_P$  Christensen & Mooney, 1995(). For a given crustal  $V_P$ , a higher geotherm would result in a more mafic composition calculated for the crust. For example, the calculated  $\text{SiO}_2$  content decreases from  $64.54 \text{ wt. \%}$  at  $400^{\circ}\text{C}$  to  $56.60 \text{ wt. \%}$  at  $700^{\circ}\text{C}$ , for a  $V_P$  of  $6.6 \text{ km/s}$  at  $30 \text{ km}$  ( $833 \text{ MPa}$ ) (Figure 4a).

- The presence of water stabilizes hydrous minerals like amphibole, biotite, and muscovite in the crust, at the expense of anhydrous minerals like pyroxene, feldspar, and garnet (Figures 4b and S3a-c) Behn & Kelemen, 2006; Guerri et al., 2015(; ). Hydrous minerals have lower  $V_P$  than pyroxene and garnet. Thus, higher water contents assumed in the crust would result in more mafic calculated crustal compositions for the same  $V_P$  (Figure S3d). For instance, assuming crustal water contents of 0, 0.25, 0.5, 0.75, 1 and 2 wt. %, the calculated  $\text{SiO}_2$  contents of the crust would vary correspondingly to be 69.38, 66.23, 63.22, 60.24, 57.55, and 54.84 wt. %, for a crustal  $V_P$  of 6.6 km/s at 30 km and 500°C (Figure 4b).

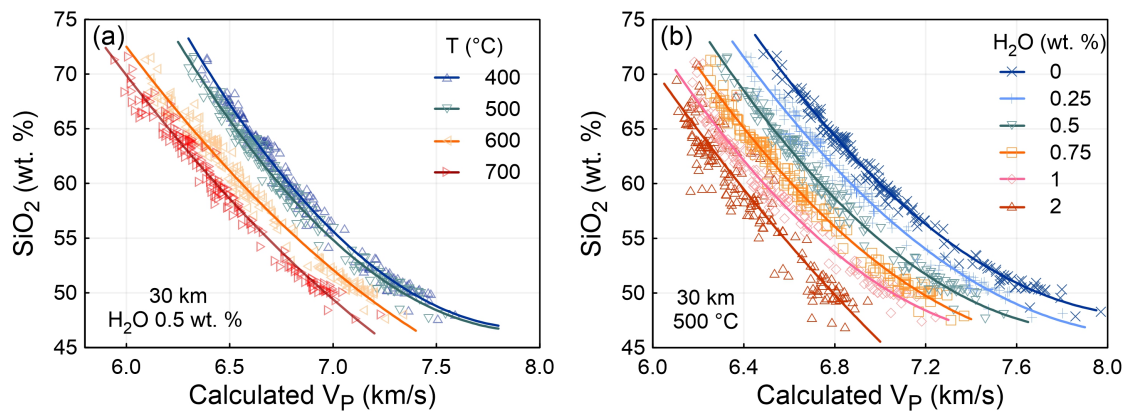


**Figure 4.** Influences of temperature (a) and assumed water content in the crust (b) on calculated  $V_P$  for mafic crustal compositions.

- Uncertainties in  $V_P$ -composition relationships are represented by RMSEs (Figure S4). Smaller RMSEs correspond to smaller uncertainties in calculated oxide contents of the crust. Typical RMSEs are about 0.9 wt. % for  $\text{SiO}_2$ , 0.7 wt. % for  $\text{CaO}$ , 0.8 wt. % for  $\text{MgO}$ , 0.9 wt. % for  $\text{FeO}_T$ , 0.45 wt. % for  $\text{K}_2\text{O}$ , 0.4 wt. % for  $\text{Na}_2\text{O}$ , 1.0 wt. % for  $\text{Al}_2\text{O}_3$ , and 0.16 wt. % for  $\text{TiO}_2$ . Uncertainties in phase equilibrium and wave speed calculations by using `Perple_X` are difficult to assess at present Connolly & Kerrick, 2002(). In this regard, we can only use the latest thermodynamic dataset, solution models, and elastic modulus of minerals to minimize the potential uncertainties.

Here we assumed that crustal  $V_P$  is only controlled by crustal composition, mineral assemblage, pressure, and temperature. Other factors such as the microfabrics (e.g., anisotropy, porosity, and the presence of liquid phase) in the crust may potentially influence the wave speeds of the crust Almquist & Mainprice, 2017(), which were not considered in this and early studies that inverting  $V_P$  to crustal compositions (e.g., Christensen and Mooney, 1995; Rudnick and Fountain, 1995; Gao et al., 1998a). The influence of these factors should be investigated in future studies.

In summary, in addition to RMSEs of  $V_P$ -composition regression, other uncertainties from our method mostly depend on crustal  $V_P$ , temperature, and water content. An increase of 0.2 km/s in observed  $V_P$ , 100°C in temperature, and 0.25 wt. % in water content would result in a decrease of about 5.28 (500°C, Figure 4a), 2.65 (6.6 km/s, Figure 4a), and 2.96 (6.6 km/s, 0–1 wt. % H<sub>2</sub>O, Figure 4b) wt. % in the estimated SiO<sub>2</sub> content of the crust, respectively. The uncertainty in estimated crustal composition could be lowered, if provided better constraints on these parameters, such as better constraints on local geotherms from xenolith studies e.g., Goes et al., 2020() or constraints on H<sub>2</sub>O content in the crust e.g., Xia et al., 2019().

### 3 Lower Crustal Compositions in Type Sections and North China Craton

Here we apply our method to two examples: the global lower crust in typical tectonic settings and the North China Craton (NCC). The geological backgrounds, physical properties, and inverted compositions of the crust for both applications are introduced below.

#### 3.1 Global Lower Continental Crust

Rudnick and Fountain (1995) compiled wave speed profiles of the lower continental crust and surface heat flow in typical tectonic settings to constrain the lower crustal compositions. They considered eight tectonic settings, including Precambrian platforms and shields, Paleozoic orogens, Mesozoic-Cenozoic extensional settings, Mesozoic-Cenozoic contractional orogens, continental arcs, active rifts, rifted margins, and forearcs.

##### 3.1.1 Geophysical and Geochemical Models of the Lower Continental Crust

The eight crustal type sections show large variations in average crustal thickness and lower crustal  $V_P$  (Figure 5a; Rudnick and Fountain, 1995). They can be classified into three groups to the average crustal thickness. Note that the average thickness and  $V_P$  below are for the bulk crust and the lower crust, respectively. (1) The thin-crust group includes rifted margins (26 km and  $V_P = 7.05$  km/s), forearcs (26 km and 6.95 km/s), active rifts (28 km and 6.77 km/s), and Mesozoic-Cenozoic extensional settings (31 km and 6.66 km/s). The type sections of these settings have a relatively thin crust (< 32 km). (2) The normal-crust group has average crustal thicknesses of 35–44 km, including Paleozoic orogens (35 km and 6.81 km/s), continental arcs (40 km and 6.92 km/s), and Precambrian platforms and shields (43 km and 7.03 km/s). (3) The thick-crust group includes only Mesozoic-Cenozoic contractional orogens (52 km and 6.71 km/s).

Rudnick and Fountain (1995) combined lower crustal  $V_P$  with  $V_P$ -composition relationships of typical lower-crustal lithologies to derive the lower crustal composition (Figure 5b and Table 1). In the estimations of Rudnick and Fountain (1995), continental arcs and rifted margins share similar mafic compositions in the lower crust ( $\text{SiO}_2$  52 wt. %), Paleozoic orogens and active rifts share similar intermediate compositions ( $\text{SiO}_2$  56 wt. %), Mesozoic-Cenozoic contractional orogens and extensional settings share similar and more felsic compositions ( $\text{SiO}_2$  59 wt. %). Considering the contribution of each tectonic setting to the global continental crust, the  $\text{SiO}_2$  of the global lower continental crust was estimated to be 53.48 wt. % (Rudnick and Fountain, 1995).

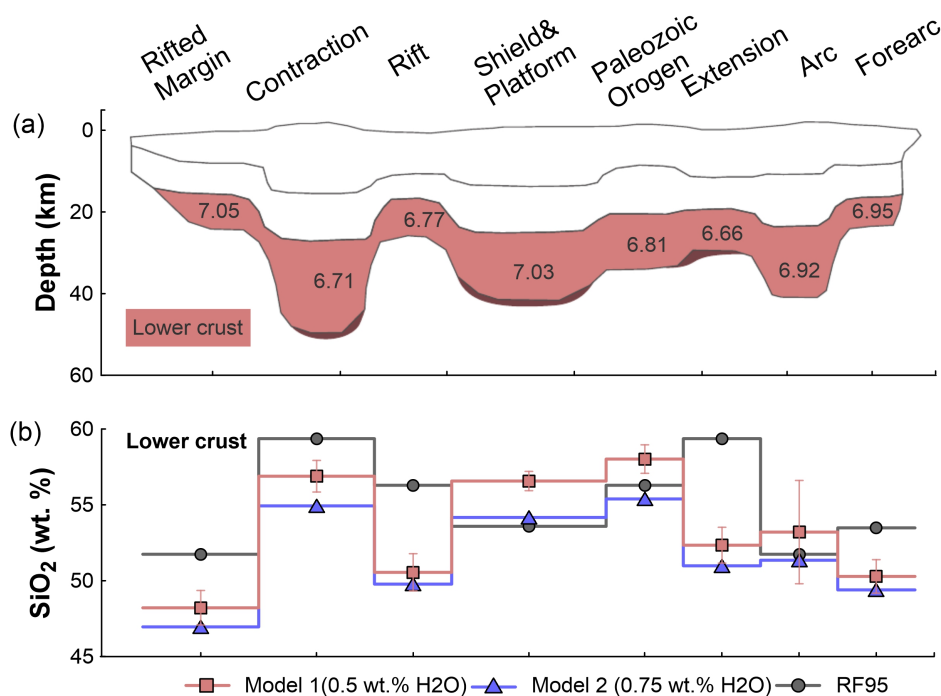


**Figure 5.** Average lower crustal  $V_P$  and  $\text{SiO}_2$  for eight typical tectonic settings in the continental crust (mo

### 3.1.2 Revisiting Lower Crustal Compositions in Different Tectonic Settings

We recalculated the lower crustal compositions for typical tectonic settings from parameters (average lower crustal  $V_P$ , crustal thicknesses, and temperatures) given in Rudnick and Fountain (1995) (Table 1). Temperatures in Rudnick and Fountain (1995) were calculated from compiled surface heat flow values assuming a steady-state thermal model Chapman & Furlong, 1992(). Pressures for the calculations correspond to the mean depth of the lower crust. Two

sets of functional relationships between  $V_P$  and oxide content were used, which assumed 0.5 and 0.75 wt. % water in the crust (the results correspond to Models 1 and 2, respectively) (Table 1). The RMSE of  $V_P$ -composition regression was used as the uncertainties in the calculated lower crustal compositions. Model 1 gave intermediate lower crustal compositions for thick- and normal- crust tectonic settings ( $\text{SiO}_2 = 56.70\text{--}58.14 \pm 0.87$  wt. %) except for continental arcs ( $53.33 \pm 3.41$  wt. %). This model gave more mafic compositions for all thin-crust settings ( $48.34\text{--}52.47 \pm 1.17$  wt. %) (Table 1; Figure 5b). In comparison, Model 2 gave more mafic compositions ( $0.77\text{--}2.63$  wt. % lower in  $\text{SiO}_2$ ) than Model 1 for all tectonic settings (Figure 5b).

Compared to the models in Rudnick and Fountain (1995), both Models 1 and 2 gave similar  $\text{SiO}_2$  for tectonic settings in the normal-crust group: shields and platforms ( $56.70 \pm 0.63$  and  $54.30 \pm 0.82$  wt. % in Models 1 and 2 vs.  $53.58$  wt. % in Rudnick and Fountain, 1995), Paleozoic orogens ( $58.14 \pm 0.94$  and  $55.51 \pm 1.04$  vs.  $56.29$  wt. %), and continental arcs ( $53.33 \pm 3.41$  and  $51.46 \pm 3.80$  vs.  $51.74$  wt. %). However, both Models 1 and 2 gave more mafic lower crustal compositions for tectonic settings with thin or thick crusts: rifted margins ( $48.34 \pm 1.14$  and  $47.09 \pm 1.41$  vs.  $51.74$  wt. %  $\text{SiO}_2$ ), active rifts ( $50.68 \pm 1.23$  and  $49.91 \pm 1.45$  vs.  $56.29$  wt. %), forearcs ( $50.42 \pm 1.11$  and  $49.52 \pm 1.35$  vs.  $53.50$  wt. %), Mesozoic-Cenozoic extensional settings ( $52.47 \pm 1.18$  and  $51.11 \pm 1.61$  vs.  $59.37$  wt. %), and Mesozoic-Cenozoic contractional orogens ( $57.01 \pm 1.04$  and  $55.04 \pm 1.53$  vs.  $59.37$  wt. %). Models 1 and 2 gave estimated  $\text{SiO}_2$  contents of  $54.41 \pm 1.01$  wt. % and  $52.57 \pm 1.24$  wt. % for the global average lower continental crust, respectively, which are similar to the estimated value of  $53.48$  wt. % in Rudnick and Fountain (1995) (Table 1).

**Table 1.** *Estimated Lower Crustal Compositions (in wt. %) for Different Tectonic Settings.* <sup>a</sup> Data from Rudnick and Fountain (1995), referred to as RF95. Models 1 and 2 were calculated from  $V_P$ -composition relationships that assume 0.5 and 0.75 wt. %  $\text{H}_2\text{O}$  in the crust, respectively. <sup>b</sup>  $\text{FeO}_T = \text{total FeO}$ . <sup>c</sup> RMSE is the root mean square error inherited from  $V_P$ -oxides regression. <sup>d</sup> A value read from Figure 14 in Rudnick and Fountain (1995).

	Tectonic	Area <sup>a</sup>	Moho <sup>a</sup>	$V_P$ <sup>a</sup>	Mean depth of the lower crust <sup>a</sup>	T <sup>a</sup>	Model
	Settings <sup>a</sup>	(%)	(km)	(km/s)	(km)	(°C)	
Thin-crust	Rifted margins	30	26	7.05	20	427	RF95 <sup>a</sup> Model RMSE Model RMSE
	Forearcs		26	6.95	21	360	RF95 <sup>a</sup> Model RMSE Model RMSE

	Tectonic	Area <sup>a</sup>	Moho <sup>a</sup>	V <sub>P</sub> <sup>a</sup>	Mean depth of the lower crust <sup>a</sup>	T <sup>a</sup>	Model
	Active rifts	1	28	6.77	21	570	RF95 <sup>a</sup> Model RMSE Model RMSE
	Mesozoic-Cenozoic extensional settings	3	31	6.66	24	663	RF95 <sup>a</sup> Model RMSE Model RMSE
Normal-crust	Paleozoic orogens	8	35	6.81	28	465	RF95 <sup>a</sup> Model RMSE Model RMSE
	Continental arcs	6	40	6.92	33	829	RF95 <sup>a</sup> Model RMSE Model RMSE
	Platforms/shields	50	43	6.98	33	461	RF95 <sup>a</sup> Model RMSE Model RMSE
Thick-crust	Mesozoic-Cenozoic contractional orogens	2	52	6.71	38	749	RF95 <sup>a</sup> Model RMSE Model RMSE
	Global lower continental crust	100					RF95 <sup>a</sup> Model RMSE Model RMSE

### 3.2 North China Craton

The North China Craton (NCC) is one of the major cratons in eastern Eurasia. The NCC is bounded by the Central Asian Orogenic Belt to the north, the Qilianshan-Qinling-Dabie Orogen to the southwest, and the Sulu-Rimjingang Orogen to the southeast Wu et al., 2018(). The NCC consists of three blocks: Western Block (WB), Trans-North China Orogen (TNCO), and Eastern Block (EB) (Figure 6a). Before the Paleozoic, the NCC was characterized by a thick,

ancient, refractory, and cold lithospheric mantle, which was considered as a defining feature of a stable craton Gao et al., 2002Griffin et al., 1998Menzies et al., 1993Xu, 2001(e.g., ; ; ; ). Since the Mesozoic, the eastern part of the NCC has been tectonically reactivated, manifested by magmatism, deformation, and replacement of the subcontinental lithospheric mantle by the asthenospheric mantle Wu et al., 2018Zhang et al., 2014Zhu et al., 2012(; ; ).

### 3.2.1 The Seismic Structure of North China Craton

A large number of geophysical explorations have been carried out in the NCC Duan et al., 2016Li et al., 2006Teng et al., 2013Xia et al., 2017(e.g., ; ; ; ). Jia et al. (2014) reported a deep seismic sounding profile across the NCC based on wide-angle reflection/refraction measurements, providing a detailed 2-D  $V_P$  structure of the crust (Figure 6a). Jia et al. (2014) divided the crust into four layers: the sedimentary layer, the upper crust, the middle crust, and the lower crust based on seismic phases. This seismic profile shows features (e.g., crustal thickness and internal structure) consistent with other regional seismic studies Xia et al., 2017(). Along the profile of Jia et al. (2014), crustal thicknesses decrease from 39–41 km in the WB to 28–32 km in the EB with a rapid transition beneath the TNCO (Figure 6a). The thickness of the lower crust decreases from ~18 km to 11–13 km from west to east. The lower crustal  $V_P$  is mostly  $< 6.9$  km/s along the profile, varying from 6.5–6.9 km/s through ~ 6.2–6.9 km/s to ~ 6.4–6.9 km/s from west to east (Figure 6a).

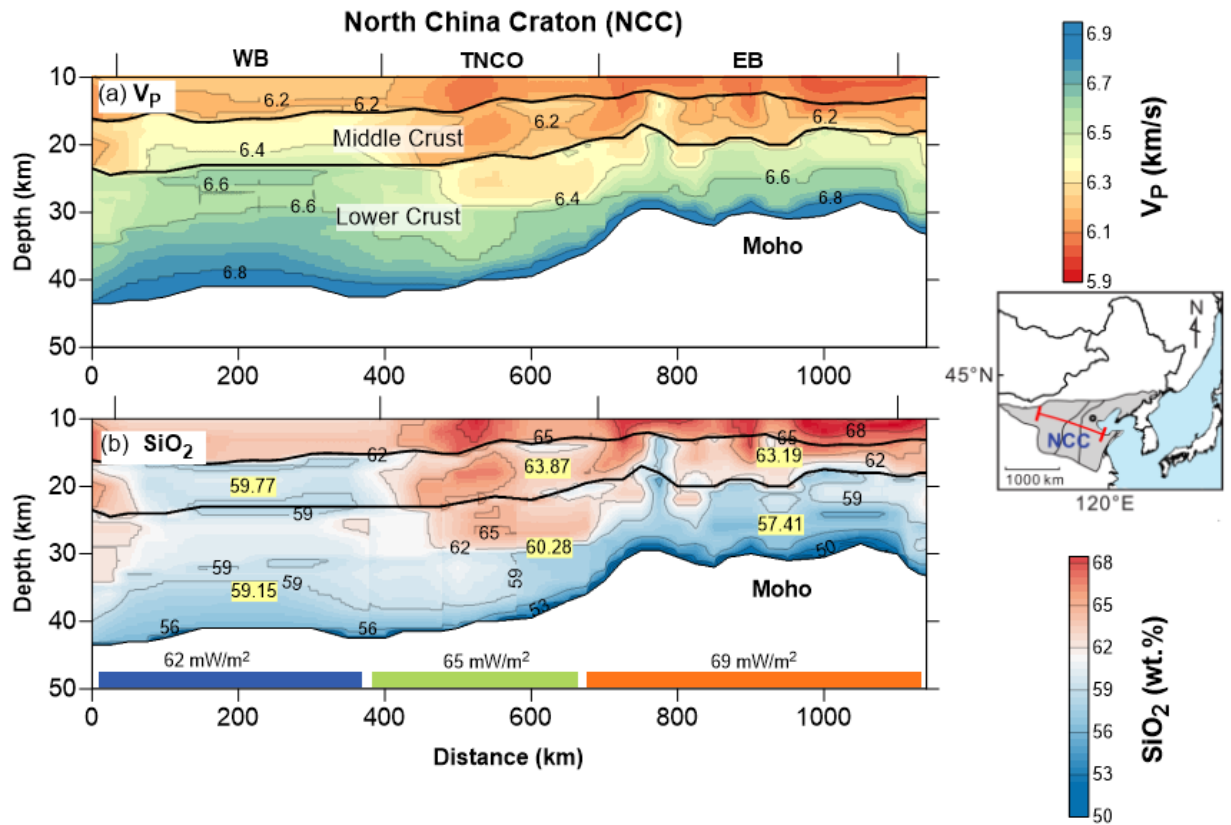


**Figure 6.** Seismic wave speed (modified from Jia et al., 2014) (a) and inferred  $\text{SiO}_2$  content (b) of the North

### 3.2.2 Inverting the Chemical Structure of the North China Craton

Local geotherms were calculated before selecting the  $V_P$ -composition relationships along the geotherm. Surface heat flow data of the NCC have been compiled by Liu et al. (2016) and Jiang et al. (2019). Average heat flow values of 62, 65, and 69 mW/m<sup>2</sup> were used in this study for the WB, TNCO, and EB, respectively (Figure 6b). Radiogenic heat production ( $A$ ) values of 1.08, 1.1, and 0.3 W/m<sup>2</sup> were used for the sedimentary layer, upper-middle crust, and lower crust, respectively. These  $A$  values were calculated from the abundances of heat production elements in >10,000 rocks from the NCC Chi & Yan, 1998(). Values of 2.2, 2.56, and 2.6 W/m/K were used for the corresponding thermal conductivities ( $k$ ) Chi & Yan, 1998Govers & Wortel, 1993(; ). The lower continental crust likely contains less water than the middle crust due to higher metamorphic grades Hacker et al., 2015(). Thus, the amounts of water in the middle and lower crust were assumed to be 0.75 and 0.5 wt. %, respectively.

Functional  $V_P$ -composition relationships along the geotherms were used to cal-

culate the crustal composition of NCC (Figure 6b). Vertically, the crust becomes more mafic with depth. The inferred  $\text{SiO}_2$  content decreases from 62 wt. % at 10 km to 56 wt. % in the lowermost crust beneath the WB, from 66 to 53 wt. % beneath TNCO, and from 66 to 50 wt. % beneath the EB. Horizontally, the middle crust beneath the WB is more mafic (average  $\text{SiO}_2 = 59.77$  wt. %) than that beneath the TNCO and EB (63.87 and 63.19 wt. %, respectively). However, the lower crust is the most mafic beneath the EB ( $\text{SiO}_2 = 57.41$  wt. %). The lowermost crust (~3 km thick) beneath the EB has 50–56 wt. %  $\text{SiO}_2$ . Overall, the WB, TNCO, and EB have similar compositions in the deep continental crust with 59.33, 61.39, and 59.37 wt. %  $\text{SiO}_2$ , respectively. The average RMSEs for the middle, lower, and deep crustal  $\text{SiO}_2$  are 1.56, 0.97, and 1.26 wt. % respectively.

## 4 Discussion

### 4.1 Chemical Models for Global Lower Continental Crust

The lower crustal composition models from Rudnick and Fountain (1995) (referred to as RF95) are the most widely accepted (Rudnick & Gao 2003, 2014). Therefore, we compare the results in this study to RF95 and then discuss the cause of differences.

Most oxide contents for the average lower continental crust in this study are consistent with RF95 within  $\pm 10\%$  difference, except for  $\text{K}_2\text{O}$  (Table1, Figure 7). The  $\text{SiO}_2$  contents for average lower crust Models 1 and 2 are 54.41 and 52.57 wt. %, respectively, while that in RF95 is 53.48 wt. %. The  $\text{K}_2\text{O}$  contents in Models 1 and 2 (0.71 and 0.98 wt. %) are higher than RF95 (0.61 wt. %). The higher values are more consistent with a recently updated  $\text{K}_2\text{O}$  value ( $0.78_{-0.21}^{+0.41}$  wt. %) for the lower continental crust based on heat-producing elements and associated geoneutrino fluxes Huang et al., 2013().

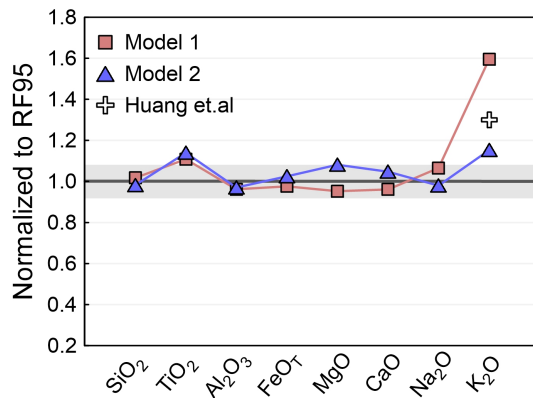


**Figure 7.** Normalized average lower continental crustal compositions estimated in this study. The oxide content

Among the eight tectonic settings, differences in estimated lower crustal  $\text{SiO}_2$  between Model 1 and RF95 range from -6.90 to +3.40 wt. %, while those between Model 2 and RF95 vary from -8.26 to +0.72 wt. % (this study minus RF95, Figure 8). The absolute differences are lowest for tectonic settings with normal crustal thicknesses (3.12 wt. % for the maximum differences): Precambrian shields and platforms (3.12 and 0.72 wt. % difference in Models 1 and 2 minus RF95), Paleozoic orogens (1.85 and -0.78 wt. %), and continental arcs (1.59 and -0.28 wt. %). However, the absolute differences are larger for tectonic settings with thin or thick crusts (-8.26 wt. % for the maximum differences). Models 1 and 2 uniformly gave more mafic compositions than RF95: rifted margins (-3.40 and -4.65 wt. % difference in Models 1 and 2 minus RF95), active rifts (-5.61 and -6.38 wt. %), forearcs (-3.08 and -3.98 wt. %), Mesozoic-Cenozoic contractional orogens (-2.36 and -4.33 wt. %), and most different in Mesozoic-Cenozoic extensional settings (-6.90 and -8.26 wt. %) (Figure 8).

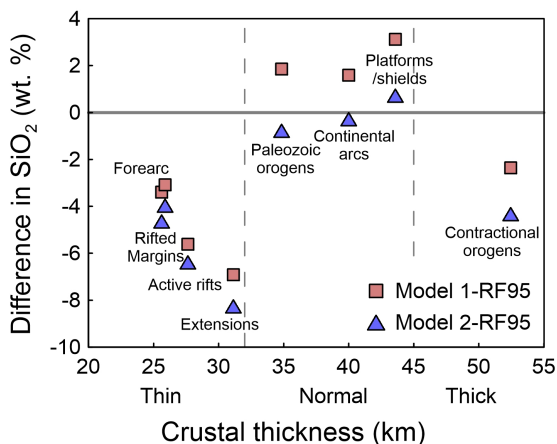


**Figure 8.** Difference in lower crustal  $\text{SiO}_2$  between this study and Rudnick and Fountain (1995) (RF95). The

Lower crust properties (e.g. seismic wave speed, pressure, and temperature) used to derive the composition are the same in this study and Rudnick and Fountain (1995). Thus, the discrepancy in estimated composition (predominantly in the thin and thick crust, Figure 8) results from the method for deriving the composition, including (1) choice of endmember lithologies in lower crust, and (2) linearly extrapolated  $V_P$ .

1. Rudnick and Fountain (1995) and several other studies (e.g., Christensen and Mooney, 1995; Kern et al., 1999; Gao et al., 2000) assessed lower crustal composition by comparing  $V_P$  of the crust to laboratory-measured  $V_P$  of natural rocks as idealized endmembers. The assignment of endmem-

bers and their properties control the calculated crustal composition. When using a two-endmember mixing model, the proportion of each lithology in the crust can be solved, if the wave speeds of the crust and the two endmember lithologies were given. However, if more endmembers are assigned in the crust, the proportions of the excess lithologies have to be assumed. For example, Rudnick and Fountain (1995) used four endmember lithologies for the lower crust: 1) mafic granulites (including both garnet-free and -bearing ones, average  $V_P = 7.23$  km/s at 600 MPa at room temperature), 2) intermediate granulites (6.66 km/s), 3) felsic granulites (6.53 km/s), and 4) metapelites (7.09 km/s). The proportion of metapelites in the lower crust was assumed to be 10%. The proportions of intermediate and felsic granulite were assumed to be equal. Using these assumptions, Rudnick and Fountain (1995) solved for the endmember proportions of the lower crust with an average  $V_P$  of 6.9 km/s; the lower crustal would consist of 40% mafic granulites, 25% intermediate and 25% felsic granulites, and 10% metapelite. If a lower  $V_P$  was used for the mafic endmember in the lower crust (e.g., garnet-free mafic granulites, amphibolites, or gabbros), the same crustal  $V_P$  would yield a higher proportion of the mafic endmember and thus a more mafic composition for the lower crust. In thin-crust tectonic settings, garnet-poor mafic lithologies are likely more common in the lower crust (Ji et al., 2015; Nishimoto et al., 2008(; ). Therefore, using relatively low- $V_P$  endmember lithologies in the lower crust would yield more mafic lower crustal compositions, which is consistent with our estimates on the lower crustal compositions for thin-crust tectonic settings (Figure 8).

2. The linearly extrapolated  $V_P$  used in Rudnick and Fountain (1995) and other studies (e.g., Christensen and Mooney, 1995; Kern et al., 1999; Gao et al., 2000) might suffer non-equilibrium issues at P-T conditions where the measured mineral assemblage is unstable. We illustrate the potential deviation by showing the P-T pseudosection, calculated  $V_P$ , and linearly extrapolated  $V_P$  from experimentally measurement for a mafic granulite ( $\text{SiO}_2 = 49.43$  wt. %) from the Dabie orogenic belt, eastern China (Kern et al., 1999) (Figure S5). The calculated  $V_P$  varies in a non-linear way with changing mineral assemblages (Figures S5a and b), which are significantly different from the linear extrapolated values (Figure S5c). The calculated and extrapolated  $V_P$  are most consistent in P-T ranges where the calculated mineral assemblage resembles that observed in the granulite (purple polygons in Figure S5), peak metamorphic condition (dashed purple boxes in Figure S5), and lower P-T regions ( $V_P$  difference  $< 0.2$  km/s). The difference between calculated and extrapolated  $V_P$  can be larger towards higher pressure and/or temperature (Figures S5b and c), which P-T condition corresponds to the lower part of thickened or hot crusts, like tectonic settings with thick and thin crust in Figure 8.

## 4.2 Implications on Growth and Evolution Mechanisms of the Continental Crust

In this study, the subduction-related (continental arcs and forearcs) and rifting-related (rifted margins, active rifts, and Mesozoic-Cenozoic extension) settings in our recalculations have mafic lower crusts ( $\text{SiO}_2 = 47.09\text{--}53.33 \pm 1.77$  wt. %) (Table 1). Subduction-related processes are central to the creation of continental crust and have been intensely studied (Ducea et al., 2015; Hacker et al., 2011; Jagoutz & Behn, 2013; Jagoutz & Kelemen, 2015; Kelemen & Behn, 2016 (e.g., ; ; ; ; )), which likely account for 60–80% of continental additions (Spencer et al., 2017). Exposed arc crustal section lithological studies also indicate mafic-ultramafic lower crust in both the continental (North American and Andean arc, average 44.78 wt. %  $\text{SiO}_2$ ; Ducea et al., 2015) and island arcs (Talkeetna and Kohistan arc, average 47.9 and 51.4 wt. %  $\text{SiO}_2$ ; Jagoutz & Kelemen, 2015). Rifting-related settings, large igneous provinces, and hotspot magmatism account for the remainder of continental additions (Spencer et al., 2017). Extension of continental lithosphere leads to the formation of rifts, extension areas, continental shelves, and ultimately to new oceanic crust (Ruppel, 1995). Extensional settings like the southern Basin and Range have a thin crust (27 km) and mafic deep crustal composition (51.2 wt. %  $\text{SiO}_2$ ), as indicated from local xenoliths and seismic data (Sammon et al., 2020). Therefore, in subduction and rifting-related settings, the additions of mantle-derived mafic magmas would contribute to the juvenile mafic crust in their lower crust (Pirajno, 2007; Spencer et al., 2017( ; ).

In contrast to subduction and rifting-related settings, Precambrian shields and platforms (also referred to as cratons) and orogens (e.g., Paleozoic orogens and Mesozoic-Cenozoic contractional orogens) have more evolved lower crust (average  $\text{SiO}_2 = 54.30\text{--}58.14 \pm 1.04$  wt. %, Figure 5b). Cratons are characterized by longevity and stability during its evolutionary history (Wu et al., 2018). They are critical for studying the evolution mechanism of continental crust, because they take up a large surface fraction of the continental crust (50%, Table 1). Xenoliths, crustal sections, and seismic studies show that diverse compositions between different cratons (e.g., more evolved compositions in the Yilgarn, Kaapvaal, and North China cratons than the Wyoming craton and Baltic shield) (Rudnick & Gao 2003, 2014). In lower-crustal xenolith suites for the Baltic shield, mafic granulites are dominant, but they appear to be absent in the Kaapvaal craton (Rudnick & Gao 2003, 2014). In all tectonic settings, orogens tend to have the most felsic lower crustal compositions (Figure 5b). Orogenesis form mountain belts such as the Alps or Himalayas at continental collision zones, or form volcanic mountain chains such as the Andes at subduction zones (Johnson & Harley, 2012). Low velocities have been observed in the orogenic crust, such as  $V_P < 6.7$  km/s for the whole 80 km thick crust of Lhasa Terrane in Tibet (Wang et al., 2021). This is potentially explained as more felsic compositions within the orogenic crust (Wang et al., 2021).

Our recalculations from averaged seismic wave speeds show that the crust in

tectonic settings where continental growth takes place (i.e., subduction and rifting-related settings), has mafic lower crustal compositions, while the crust in other tectonic settings (i.e., cratons and orogens) tend to have more evolved compositions. The classical Wilson cycle suggests that the history of the continental crust can be broken into five stages, including rift, passive margin, subduction, accretion, and continent-continent collision Wilson, 1968(). Classic models for orogens in Wilson cycle imply that orogenesis occurs at the end of the cycle of oceanic opening and closing with continent-continent collision Cawood et al., 2022(). Subsequently, cratonization of the continents results in differentiation-stratification of the stable upper and lower crust, as well as attaining crust-mantle coupling Zhai, 2011(). Our results show that cratons and orogens have more felsic compositions in the lower crust than supra-subduction zones and rifting-related regions, which indicates that cratons and orogens have evolved to relatively mature conditions during/after orogenesis and cratonization processes, at least from the composition perspective. These processes are important for the continental crust to possess an average andesitic bulk composition.

### 4.3 The Chemical Structure of North China Craton and Implications

Here we compare our results with previous interpretations of the NCC. We further interpret the obtained 2-D chemical structure of the NCC in light of a geologic context.

The crustal composition of the NCC has been investigated by studying the lower crustal xenoliths and seismic wave speed structures of the crust (e.g., Gao et al., 1998a, 1999, 1998b; Kern et al., 1996; Liu et al., 2001). Gao et al. (1998a, 1999, 1998b) studied the crustal composition in East China (mainly the NCC and the Qinling orogenic belt to the south) by comparing seismic data from regional seismic refraction profiles to measured wave speeds of natural samples considering typical lower crustal rocks. Their results show two seismic and chemical layers of the lower crust in East China: an upper lower crust that is featured by  $V_P = 6.7$  km/s and an intermediate (57–66 wt. %  $\text{SiO}_2$ ) composition, and a lowermost crust (3–5 km thick at the base) having  $V_P = 7.1$  km/s and a mafic composition (50 wt. %  $\text{SiO}_2$ ). Gao et al. (1999) estimated intermediate bulk lower crust (58 wt. %  $\text{SiO}_2$ ) after weighted averaging in the East China. A xenolith study shows that granulite xenoliths entrapped by Cenozoic basalts from the northern TNCO have mafic to felsic compositions with  $\text{SiO}_2$  ranging from 45.7 to 73.0 wt. % (Liu et al., 2001). Forty-five percents of these granulites have intermediate to felsic compositions (Liu et al., 2001). By integrating thermobarometric P-T estimations, calculated  $V_P$  of lower crustal granulites, and regional seismic refraction results, Liu et al. (2001) also suggested a two-layer model for the lower crust in the TNCO and an average bulk crustal  $\text{SiO}_2$  of 58 wt. %.

Our estimated crustal compositions (Figure 6) are consistent with the inter-

media compositions suggested in previous studies. The average lower crustal composition of the TNCO and EB is intermediate in this study ( $60.28$  and  $57.41 \pm 0.97$  wt. %  $\text{SiO}_2$ ) (Figure 6). Along the whole profile, the crust with  $V_p > 7.1$  km/s has mafic compositions ( $\text{SiO}_2 < 52$  wt. %) (Figure S6), which supports the conclusion of Behn and Kelemen (2003) and Hacker et al. (2015) that a crust with  $V_p > 7.2$  km/s must be mafic. Our analysis also agrees with previous two-layer lower crustal models of the NCC based on xenolith and seismic structures (Gao et al., 1998a, 1999, 1998b; Liu et al., 2001). The two-layer lower crust is most apparent beneath the EB (Figure 6b). The shallow lower-crustal layer of the EB is 8 km thick with an average of  $\sim 58$  wt. %  $\text{SiO}_2$  and the deeper lower-crustal layer is 3 km thick with an average of  $\sim 53$  wt. %  $\text{SiO}_2$ . Towards the west, this mafic deeper layer becomes thinner beneath the TNCO and almost absent beneath the WB (Figure 6b).

The seismic and our estimated chemical structures of the NCC show heterogeneity from the west to the east (Figure 6). The EB is characterized by a thin crust (30 km in thickness), which is 10 km thinner than the WB (40 km in thickness). Besides, the EB has a more felsic middle crust (average 63.19 vs.  $59.77 \pm 1.56$  wt. %  $\text{SiO}_2$ ) and more mafic lower crust than the WB (average 57.41 vs.  $59.15 \pm 0.97$  wt. %  $\text{SiO}_2$ ), especially at the lowermost part (Figure 6b). The EB has a heterogeneous lower crust, while the WB has a more homogeneous chemical structure (Figure 6). While both EB and WB are Precambrian cratons, the large difference in the interpreted chemical structure likely results from their different tectonic histories in the Phanerozoic. The WB is considered to be stable and rigid, and retained the characteristics of a typical craton ( a  $\sim 200$  km thick lithosphere) Chen et al., 2009(). In contrast, the EB is a destructed craton with a thin lithosphere ( $\sim 80$  km) Wu et al., 2018(). Besides, the EB has interlaced and nonuniform chemical layering, and a mafic lower-most crust (Figure 6b). These compositional features are consistent with intensive magmatism and asthenosphere upwelling during Mesozoic-Cenozoic extension and lithospheric thinning induced by the rollback of the Pacific Plate Gao et al., 2004Ma & Xu, 2021Wu et al., 2018Zhu & Xu, 2019(; ; ; ). Thus, we interpret the chemical variation and layering within the EB to be the combined result of Mesozoic crustal thickening, removal of the dense lithospheric root, and mantle magmatism Ju et al., 2021Zhu et al., 2012(; ; ).

The spatial composition distribution of the NCC indicates the deep crust compositions in the orogenic crust (TNCO) is the most felsic of the three units (average  $63.87 \pm 1.56$  and  $60.28 \pm 0.97$  wt. %  $\text{SiO}_2$  for the middle and lower crust; Figure 6b). The evolution of TNCO was mainly controlled by the Paleoproterozoic continental collision followed by Mesozoic and Cenozoic folding, uplift, and extensional detachment Ju et al., 2021(). In contractional orogens, partial melting and differentiation of the continental crust can produce more felsic upper and middle crustal compositions DeCelles et al., 2009(). Crustal thickening during the building of collisional orogens causes eclogite-facies metamorphism in the lowermost crust Spencer et al., 2017(). As eclogites are denser than underlying mantle peridotites, the lowermost mafic crust can be delami-

nated Gao et al., 2004(). This process was suggested for the Altiplano-Puna Plateau in the Andes Kay et al., 1994(). Similar processes can also take place at the base of thick arcs (e.g., Sierra Nevadas) by removal of arclogites (i.e., eclogite-facies pyroxene-rich rocks formed in equilibrium with a melt) Ducea et al., 2015Lee & Anderson, 2015(; ). After the removal of dense mafic material from the lower crust, the remaining buoyant lower crust would be intermediate in composition Hawkesworth & Kemp, 2006(). For these reasons, we interpret that the TNCO has evolved to more intermediate compositions through intra-crustal differentiation combined with removal of dense mafic materials at the lowermost crust during orogenesis and extension (Zhu et al., 2012; Ju et al., 2021).

In summary, the thin crust EB has a more felsic middle crust and a more mafic lower crust compared to the WB. This difference may have been caused by more intense lithospheric delamination and asthenosphere upwelling in the eastern NCC Wu et al., 2018(). We interpret the felsic lower crust of the TNCO to be mainly influenced by intra-crustal differentiation and removal of dense eclogitic crust during orogenesis and later extension (Ju et al., 2021). The inferred chemical structure of the NCC can serve as a reference model for comparison with other cratons.

## 5 Conclusions

This paper presents a geophysical-geochemical modeling for inferring deep crustal compositional structures from crustal observed  $V_P$ . First, we compiled 172 published chemical models providing variation patterns in the continental crust composition. Secondly, functional  $V_P$ -composition relationships are established for common P-T conditions (10-80 km, 50-1200°C) from modal crustal compositions and their thermodynamically calculated  $V_P$ . The relationships are robust for oxides  $\text{SiO}_2$ ,  $\text{CaO}$ ,  $\text{FeO}_T$ ,  $\text{MgO}$ , and  $\text{K}_2\text{O}$  in the -quartz stability field ( $R^2 > 0.7$ ). We provide a MATLAB user-friendly graphical user interface (GUI) for the whole inverting process (CalcCrustComp). With the given  $V_P$ , depth, and temperature, users can invert their deep crustal composition (major oxides).

Using this geophysical-geochemical modeling, we recalculated the lower crustal compositions of typical tectonic settings in Rudnick and Fountain (1995) and inverted crustal chemical structure from a 2-D  $V_P$  profile Jia et al., 2014() across North China Craton. We found the following conclusions:

1. Our estimated compositions on the average global lower crust are mostly consistent with Rudnick and Fountain (1995) within  $\pm 10\%$  difference, except for higher  $\text{K}_2\text{O}$  content in agreement with more recent studies (Huang et al. 2013). The estimates for thin- (rifted margins, forearcs, active rifts, and extensional settings) and thick- (Mesozoic-Cenozoic contractional orogens) crust regions are more mafic than Rudnick and Fountain (1995). The

reason for these composition differences is that we avoid the empirical assignments of deep crust endmember lithologies and linearly extrapolated  $V_p$  in the previous method.

2. Our recalculations suggest mafic lower crustal compositions for subduction-related (continental arcs and forearcs) and rifting-related settings (rifted margins, active rifts, Mesozoic-Cenozoic extension) ( $47.09\text{--}53.33 \pm 1.77$  wt. %  $\text{SiO}_2$ ), and intermediate lower crustal compositions for Precambrian shields and platforms and orogens (e.g., Paleozoic orogens and Mesozoic-Cenozoic contractional orogens) ( $54.30\text{--}58.14 \pm 1.04$  wt. %  $\text{SiO}_2$ ). These observations indicate the continent has evolved to the relatively mature compositional condition after orogenesis and cratonization processes.
3. Compared to the WB, which represents the stable part of the NCC, the EB has a thinner (40 vs. 30 km) crust Jia et al., 2014() with more felsic middle crust ( $59.77$  vs.  $63.19 \pm 1.56$  wt. % average  $\text{SiO}_2$ ) and more mafic lower crust ( $59.15$  vs.  $57.41 \pm 0.97$  wt. % average  $\text{SiO}_2$ ). Moreover, a mafic lowermost layer ( $\sim 3$  km thick) in the EB is almost absent beneath the WB. These features of EB agree well with compositional findings and evolution history in previous studies. The TNCO is the most felsic in all units ( $63.87 \pm 1.56$  and  $60.28 \pm 0.97$  wt. % average  $\text{SiO}_2$  for the middle and lower crust), which agrees with the evolution history of intra-crustal differentiation combined with the removal of dense mafic materials from the lowermost crust.

Our modeling provides an efficient way to construct crustal chemical structures from crustal wave speed structures. Although with simplifications, the estimated composition from this modeling can serve as a reference model, from which crustal heterogeneity can be identified. Admittedly, the sources of uncertainty in the inverted chemical composition of the crust are multifold, but can be constrained by regional geology and geophysics. Future studies are also needed on the influence of microfabrics on the seismic wave speed of the crust, which are not addresses in this study.

## Acknowledgments

This study was supported by the National Natural Science Foundation of China (Nos. 41730211, 42130307, and 41973024), the National Key Research and Development Project of China (No. 2016YFC0600309), the 111 Project (No. BP0719022), the MOST Special Fund from State Key Laboratory of Geological Processes and Mineral Resources (Nos.GPMR202002 and MSFGPMR02-1), and the National Science Foundation Grant EAR 19-52642.

## Data and software availability statement

The data and MATLAB GUI code (CalcCrustComp) supporting these conclusions can be found at <https://zenodo.org/record/7043354?token=eyJhbGciOiJIUzUxMiIsImV4cCI6MTY2NDc0Nzk5OSwiaWF0IjoxNjYyMTI2NDQ4fQ.eyJkYXRhIjp7InJlY2lkIjo3MDQzMzU0fSwiaWQiOiI1NzczLCJyb291I3ZjMyNDk1MiJ9.XDbyA87W6mjW8uBcANnnnwdJVU9KBCieHvOgFTRDbkOgzLS2SipMvIImSlNbeQbkX-SWZtv9ljGeJ-3T51JqdA>

(temporary private link)

## References

- <https://doi.org/10.1002/2015gc006171>
- <https://doi.org/10.1002/2016rg000552>
- [https://doi.org/10.1016/0040-1951\(89\)90154-6](https://doi.org/10.1016/0040-1951(89)90154-6)
- <https://doi.org/10.1016/j.epsl.2019.01.033>
- <https://doi.org/10.1029/2002gc000393>
- <https://doi.org/10.1029/2006jb004327>
- <https://doi.org/10.1144/sp318.1>
- <https://doi.org/10.1144/gsl.sp.1986.024.01.07>
- <https://doi.org/10.1016/j.epsl.2009.06.022>
- <https://doi.org/10.1088/0256-307X/16/9/027>
- <https://doi.org/10.1029/95jb03446>
- <https://doi.org/10.1029/95jb00259>
- <https://doi.org/10.1029/2009gc002540>
- [https://doi.org/10.1016/S0012-821X\(02\)00957-3](https://doi.org/10.1016/S0012-821X(02)00957-3)
- <https://doi.org/10.1038/ngeo469>
- <https://doi.org/10.1002/2016tc004405>
- <https://doi.org/10.1007/s11430-016-5301-0>
- <https://doi.org/10.1146/annurev-earth-060614-105049>
- <https://doi.org/10.1029/2000jb900100>
- [https://doi.org/10.1016/S0016-7037\(98\)00121-5](https://doi.org/10.1016/S0016-7037(98)00121-5)

<https://doi.org/10.1007/BF02878511>  
[https://doi.org/10.1016/S0012-821X\(02\)00489-2](https://doi.org/10.1016/S0012-821X(02)00489-2)  
<https://doi.org/10.1038/nature03162>  
[https://doi.org/10.1016/S0012-821X\(98\)00140-X](https://doi.org/10.1016/S0012-821X(98)00140-X)  
<https://doi.org/10.1016/j.pepi.2020.106509>  
[https://doi.org/10.1016/0040-1951\(93\)90159-H](https://doi.org/10.1016/0040-1951(93)90159-H)  
<https://doi.org/10.1111/jmg.12211>  
<https://doi.org/10.1002/2015gc005819>  
<https://doi.org/10.1007/s00410-020-01696-y>  
<https://doi.org/10.1016/j.epsl.2011.05.024>  
<https://doi.org/10.1146/annurev-earth-050212-124117>  
<https://doi.org/10.1016/j.chemgeo.2005.09.017>  
<https://doi.org/10.1007/s00410-003-0464-z>  
<https://doi.org/10.1111/j.1525-1314.1998.00140.x>  
<https://doi.org/10.1111/j.1525-1314.2010.00923.x>  
<https://doi.org/10.1130/g38619.1>  
<https://doi.org/10.1002/ggge.20129>  
<https://doi.org/10.1038/nature12758>  
<https://doi.org/10.1146/annurev-earth-040809-152345>  
<https://doi.org/10.1016/j.chemgeo.2011.10.022>  
<https://doi.org/10.1002/2015jb012209>  
<https://doi.org/10.1016/j.tecto.2014.04.013>  
<https://doi.org/10.1016/j.tecto.2019.01.006>  
<https://doi.org/10.1016/j.epsl.2007.11.045>  
<https://doi.org/10.1016/j.earscirev.2021.103859>  
<https://doi.org/10.1029/94jb00896>  
<https://doi.org/10.1038/Ngeo2662>  
<https://doi.org/10.1126/science.1174156>

[https://doi.org/10.1016/0012-821x\(95\)00240-d](https://doi.org/10.1016/0012-821x(95)00240-d)  
[https://doi.org/10.1016/0031-9201\(85\)90126-8](https://doi.org/10.1016/0031-9201(85)90126-8)  
<https://doi.org/10.1007/s11434-015-0828-6>  
<https://doi.org/10.1126/science.1217313>  
<https://doi.org/10.1016/j.tecto.2006.01.026>  
<https://doi.org/10.1016/j.jog.2016.09.005>  
[https://doi.org/10.1016/S0016-7037\(01\)00609-3](https://doi.org/10.1016/S0016-7037(01)00609-3)  
<https://doi.org/10.1016/j.earscirev.2020.103473>  
<https://doi.org/10.1016/b978-0-444-53802-4.00010-5>  
<https://doi.org/10.1029/2008jb005587>  
[https://doi.org/10.1016/S0166-2635\(07\)15083-0](https://doi.org/10.1016/S0166-2635(07)15083-0)  
<https://doi.org/10.1115/1.3138643>  
<https://doi.org/10.1016/B0-08-043751-6/03016-4>  
<https://doi.org/10.1016/B978-0-08-095975-7.00301-6>  
<https://doi.org/10.1029/95rg01302>  
<https://doi.org/10.1029/JB092iB13p13981>  
<https://doi.org/10.1029/95jb02955>  
<https://doi.org/10.1029/2019jb019011>  
<https://doi.org/10.1029/2022jb024041>  
<https://doi.org/10.1144/GSL.SP.1986.024.01.24>  
<https://doi.org/10.1139/e94-099>  
<https://doi.org/10.1139/e67-058>  
<https://doi.org/10.1002/2015gl065459>  
<https://doi.org/10.1016/j.epsl.2018.04.055>  
<https://doi.org/10.1029/gl005i009p00749>  
<https://doi.org/10.1016/j.earscirev.2017.07.013>  
<https://doi.org/10.1144/gsl.sp.1989.042.01.19>

[https://doi.org/10.1016/0016-7037\(64\)90129-2](https://doi.org/10.1016/0016-7037(64)90129-2)  
<https://doi.org/10.1016/j.tecto.2012.11.024>  
<https://doi.org/10.1016/j.tecto.2013.05.032>  
<https://doi.org/10.1038/s41467-021-21420-z>  
<https://doi.org/10.1038/310575a0>  
[https://doi.org/10.1016/0016-7037\(95\)00038-2](https://doi.org/10.1016/0016-7037(95)00038-2)  
<https://doi.org/10.1046/j.1525-1314.2000.00269.x>  
<https://doi.org/10.1046/j.0263-4929.2001.00349.x>  
<https://doi.org/10.1111/jmg.12071>  
<https://doi.org/10.1016/B978-0-08-095975-7.00315-6>  
<https://doi.org/10.1016/j.chemgeo.2010.06.005>  
<https://doi.org/10.1146/annurev-earth-053018-060342>  
<https://doi.org/10.1002/2016jb013848>  
<https://doi.org/10.1093/nsr/nwx016>  
[https://doi.org/10.1016/s1464-1895\(01\)00124-7](https://doi.org/10.1016/s1464-1895(01)00124-7)  
<https://doi.org/10.1029/2019jb017741>  
<https://doi.org/10.1007/s11430-011-4250-x>  
<https://doi.org/10.1016/j.earscirev.2013.12.004>  
<https://doi.org/10.1016/j.tecto.2013.02.040>  
<https://doi.org/10.1029/2006jb004503>  
<https://doi.org/10.1016/j.gr.2019.07.010>  
<https://doi.org/10.1007/s11430-018-9356-y>  
<https://doi.org/10.1016/j.lithos.2012.05.013>

Abers, G. A., & Hacker, B. R. (2016). A MATLAB toolbox and Excel workbook for calculating the densities, seismic wave speeds, and major element composition of minerals and rocks at pressure and temperature. *Geochemistry, Geophysics, Geosystems*, *17*(2), 616-624. Almquist, B. S. G., & Mainprice, D. (2017). Seismic properties and anisotropy of the continental crust: Predictions based on mineral texture and rock microstructure. *Reviews of Geophysics*, *55*(2), 367-433. Arndt, N. T., & Goldstein, S. L. (1989). An open boundary between lower continental crust and mantle: its role in crust formation and crustal recycling. *Tectonophysics*, *161*(3-4), 201-212. Artemieva, I. M., & Shulgin, A. (2019). Making and altering the crust: A global perspective on crustal structure and evolution. *Earth and Planetary Science Letters*, *512*, 8-16. Austrheim,

H. (1998). Influence of fluid and deformation on metamorphism of the deep crust and consequences for the geodynamics of collision zones. In Hacker B. & Liou J. (Eds.), *When continents collide: Geodynamics and geochemistry of ultrahigh-pressure rocks*(pp. 297-323). Springer. Behn, M. D., & Kelemen, P. B. (2003). Relationship between seismic P-wave velocity and the composition of anhydrous igneous and meta-igneous rocks. *Geochemistry, Geophysics, Geosystems*, 4(5), 1041. Behn, M. D., & Kelemen, P. B. (2006). Stability of arc lower crust: Insights from the Talkeetna arc section, south central Alaska, and the seismic structure of modern arcs. *Journal of Geophysical Research: Solid Earth*, 111(B11207). Borodin, L. (1999). Estimated chemical composition and petrochemical evolution of the upper continental crust. *Geochemistry International*, 37(8), 723-734. Cawood, P. A., Kröner, A., Collins, W. J., Kusky, T. M., Mooney, W. D., & Windley, B. F. (2022). Accretionary orogens through Earth history. *Geological Society, London, Special Publications*, 318(1), 1-36. Chapman, D. S. (1986). Thermal gradients in the continental crust. *Geological Society, London, Special Publications*, 24(1), 63-70. Chapman, D. S., & Furlong, K. (1992). Thermal state of the continental lower crust. In Fountain D. M., Arculus R. & Kay R. W. (Eds.), *Continental lower crust*(pp. 179-200). New York, Elsevier Sci. Chen, L., Cheng, C., & Wei, Z. (2009). Seismic evidence for significant lateral variations in lithospheric thickness beneath the central and western North China Craton. *Earth and Planetary Science Letters*, 286(1-2), 171-183. Chi, Q.-H., & Yan, M.-C. (1998). Radioactive elements of rocks in North China platform and the thermal structure and temperature distribution of the modern-continental lithosphere. *Acta Geophysica Sinica*, 41(1), 38-47. Christensen, N. I. (1996). Poisson's ratio and crustal seismology. *Journal of Geophysical Research: Solid Earth*, 101(B2), 3139-3156. Christensen, N. I., & Mooney, W. D. (1995). Seismic velocity structure and composition of the continental crust: A global view. *Journal of Geophysical Research: Solid Earth*, 100(B7), 9761-9788. Clarke, F. (1889). The relative abundance of the chemical elements. *Philosophical Society of Washington Bulletin*, XI, 131-142. Clarke, F., & Washington, H. (1924). The composition of the Earth's crust. *US Geological Survey Professional Paper*, 131-142. Connolly, J. A. D. (2009). The geodynamic equation of state: What and how. *Geochemistry, Geophysics, Geosystems*, 10(Q10014). Connolly, J. A. D., & Kerrick, D. M. (2002). Metamorphic controls on seismic velocity of subducted oceanic crust at 100-250 km depth. *Earth & Planetary Science Letters*, 204(1-2), 61-74. DeCelles, P. G., Ducea, M. N., Kapp, P., & Zandt, G. (2009). Cyclicity in Cordilleran orogenic systems. *Nature Geoscience*, 2(4), 251-257. Diaferia, G., & Cammarano, F. (2017). Seismic signature of the continental crust: What thermodynamics says. An example from the Italian Peninsula. *Tectonics*, 36(12), 3192-3208. Duan, Y.-H., Wang, F.-Y., Zhang, X.-K., Lin, J.-Y., Liu, Z., Liu, B.-F., Yang, Z.-X., Guo, W.-B., & Wei, Y.-H. (2016). Three-dimensional crustal velocity structure model of the middle-eastern north China Craton (HBCrust1.0). *Science China Earth Sciences*, 59(7), 1477-1488. Ducea, M. N., Saleeby, J. B., & Bergantz, G. (2015). The architecture, chemistry, and evolution of continental magmatic arcs. *Annual Review of Earth and Planetary Sciences*, 43(1), 299-331. Gao, S., Kern, H., Liu, Y.-S., Jin, S.-Y.,

Popp, T., Jin, Z.-M., Feng, J.-L., Sun, M., & Zhao, Z.-B. (2000). Measured and calculated seismic velocities and densities for granulites from xenolith occurrences and adjacent exposed lower crustal sections: A comparative study from the North China craton. *Journal of Geophysical Research: Solid Earth*, *105*(B8), 18965-18976. Gao, S., Luo, T.-C., Zhang, B.-R., Zhang, H.-F., Han, Y.-W., Zhao, Z.-D., & Hu, Y.-K. (1998a). Chemical composition of the continental crust as revealed by studies in East China. *Geochimica et Cosmochimica Acta*, *62*(11), 1959-1975. Gao, S., Luo, T.-C., Zhang, B.-R., Zhang, H.-F., & Kern, H. (1999). Structure and composition of the continental crust in East China. *Science in China (Series D)*, *42*(2), 129-140. Gao, S., Rudnick, R. L., Carlson, R. W., McDonough, W. F., & Liu, Y.-S. (2002). Re-Os evidence for replacement of ancient mantle lithosphere beneath the North China craton. *Earth & Planetary Science Letters*, *198*(3-4), 307-322. Gao, S., Rudnick, R. L., Yuan, H.-L., Liu, X.-M., Liu, Y.-S., Xu, W.-L., Ling, W.-L., Ayers, J., Wang, X.-C., & Wang, Q.-H. (2004). Recycling lower continental crust in the North China craton. *Nature*, *432*(7019), 892-897. Gao, S., Zhang, B.-R., Jin, Z.-M., Kern, H., Luo, T.-C., & Zhao, Z.-D. (1998b). How mafic is the lower continental crust? *Earth and Planetary Science Letters*, *161*(1-4), 101-117. Goes, S., Hasterok, D., Schutt, D. L., & Klöcking, M. (2020). Continental lithospheric temperatures: A review. *Physics of the Earth and Planetary Interiors*, *306*, 106509. Govers, R., & Wortel, M. (1993). Initiation of asymmetric extension in continental lithosphere. *Tectonophysics*, *223*(1), 75-96. Green, E. C. R., White, R. W., Diener, J. F. A., Powell, R., Holland, T. J. B., & Palin, R. M. (2016). Activity-composition relations for the calculation of partial melting equilibria in metabasic rocks. *Journal of Metamorphic Geology*, *34*(9), 845-869. Griffin, W. L., Zhang, A., O'Reilly, S. Y., & Ryan, C. G. (1998). Phanerozoic evolution of the lithosphere beneath the Sino-Korean Craton. In Martin F. J. Flower S.-L. C., Ching-Hua Lo, Tung-Yi Lee (Eds.), *Mantle Dynamics and Plate Interactions in East Asia* (pp. 107-126). Washington, D. C., American Geophysical Union. Guerri, M., Cammarano, F., & Connolly, J. A. D. (2015). Effects of chemical composition, water and temperature on physical properties of continental crust. *Geochemistry, Geophysics, Geosystems*, *16*(7), 2431-2449. Guo, L., Jagoutz, O., Shinevar, W. J., & Zhang, H.-F. (2020). Formation and composition of the Late Cretaceous Gangdese arc lower crust in southern Tibet. *Contributions to Mineralogy and Petrology*, *175*(6), 1-26. Hacker, B. R., Kelemen, P. B., & Behn, M. D. (2011). Differentiation of the continental crust by reamination. *Earth and Planetary Science Letters*, *307*(3-4), 501-516. Hacker, B. R., Kelemen, P. B., & Behn, M. D. (2015). Continental lower crust. *Annual Review of Earth and Planetary Sciences*, *43*(1), 167-205. Hawkesworth, C. J., & Kemp, A. I. S. (2006). The differentiation and rates of generation of the continental crust. *Chemical Geology*, *226*(3-4), 134-143. Holland, T., & Powell, R. (2003). Activity-composition relations for phases in petrological calculations: an asymmetric multicomponent formulation. *Contributions to Mineralogy and Petrology*, *145*(4), 492-501. Holland, T. J. B., & Powell, R. (1998). An internally consistent thermodynamic data set for phases of petrological interest. *Journal of Metamorphic Geology*, *16*(3), 309-343. Holland, T. J. B., & Powell, R. (2011). An

improved and extended internally consistent thermodynamic dataset for phases of petrological interest, involving a new equation of state for solids. *Journal of Metamorphic Geology*, 29(3), 333-383. Hou, Z.-Q., Zhou, Y., Wang, R., Zheng, Y.-C., He, W.-Y., Zhao, M., Evans, N. J., & Weinberg, R. F. (2017). Recycling of metal-fertilized lower continental crust: Origin of non-arc Au-rich porphyry deposits at cratonic edges. *Geology*, 45(6), 563-566. Huang, Y., Chubakov, V., Mantovani, F., Rudnick, R. L., & McDonough, W. F. (2013). A reference Earth model for the heat-producing elements and associated geoneutrino flux. *Geochemistry, Geophysics, Geosystems*, 14(6), 2003-2029. Jagoutz, O., & Behn, M. D. (2013). Foundering of lower island-arc crust as an explanation for the origin of the continental Moho. *Nature*, 504(7478), 131-134. Jagoutz, O., & Kelemen, P. B. (2015). Role of arc processes in the formation of continental crust. *Annual Review of Earth and Planetary Sciences*, 43(1), 363-404. Jagoutz, O., & Schmidt, M. W. (2012). The formation and bulk composition of modern juvenile continental crust: The Kohistan arc. *Chemical Geology*, 298-299, 79-96. Ji, S.-C., Shao, T.-B., Michibayashi, K., Oya, S., Satsukawa, T., Wang, Q., Zhao, W.-H., & Salisbury, M. H. (2015). Magnitude and symmetry of seismic anisotropy in mica- and amphibole-bearing metamorphic rocks and implications for tectonic interpretation of seismic data from the southeast Tibetan Plateau. *Journal of Geophysical Research: Solid Earth*, 120(9), 6404-6430. Jia, S.-X., Wang, F.-Y., Tian, X.-F., Duan, Y.-H., Zhang, J.-S., Liu, B.-F., & Lin, J.-Y. (2014). Crustal structure and tectonic study of North China Craton from a long deep seismic sounding profile. *Tectonophysics*, 627, 48-56. Jiang, G.-Z., Hu, S.-B., Shi, Y.-Z., Zhang, C., Wang, Z.-T., & Hu, D. (2019). Terrestrial heat flow of continental China: Updated dataset and tectonic implications. *Tectonophysics*, 753, 36-48. Jiménez-Munt, I., Fernández, M., Vergés, J., & Platt, J. P. (2008). Lithosphere structure underneath the Tibetan Plateau inferred from elevation, gravity and geoid anomalies. *Earth and Planetary Science Letters*, 267(1-2), 276-289. Johnson, M. R. W., & Harley, S. L. (2012). Major features of the Earth and plate tectonics, *Orogenesis: The Making of Mountains*(pp. 1-9). Cambridge, Cambridge University Press. Ju, Y.-W., et al. (2021). Coupling response of the Meso-Cenozoic differential evolution of the North China Craton to lithospheric structural transformation. *Earth-Science Reviews*, 223, 103859. Kay, S. M., Coira, B., & Viramonte, J. (1994). Young mafic back arc volcanic rocks as indicators of continental lithospheric delamination beneath the Argentine Puna Plateau, central Andes. *Journal of Geophysical Research: Solid Earth*, 99(B12), 24323-24339. Kelemen, P. B., & Behn, M. D. (2016). Formation of lower continental crust by relamination of buoyant arc lavas and plutons. *Nature Geoscience*, 9(3), 197-205. Kelemen, P. B., Hanghøj, K., & Greene, A. R. (2007). One view of the geochemistry of subduction-related magmatic arcs, with an emphasis on primitive andesite and lower crust. *Treatise on Geochemistry*, 3, 1-70. Kelley, K. A., & Cottrell, E. (2009). Water and the oxidation state of subduction zone magmas. *Science*, 325(5940), 605-607. Kern, H., Gao, S., & Liu, Q.-S. (1996). Seismic properties and densities of middle and lower crustal rocks exposed along the North China Geoscience Transect. *Earth and Planetary Science Letters*, 139(3-4), 439-455. Kern, H., & Schenk, V.

(1985). Elastic wave velocities in rocks from a lower crustal section in southern Calabria (Italy). *Physics of The Earth and Planetary Interiors*, 40(3), 147-160. Lee, C.-T. A., & Anderson, D. L. (2015). Continental crust formation at arcs, the arclogite “delamination” cycle, and one origin for fertile melting anomalies in the mantle. *Science Bulletin*, 60(13), 1141-1156. Lee, C.-T. A. L., P., Chin, E. J., Bouchet, R., Dasgupta, R., Morton, D. M., Roux, V. L., Yin, Q.-Z., & Jin, D. (2012). Copper systematics in arc magmas and implications for crust-mantle differentiation. *Science*, 336(6077), 64-68. Li, S.-L., Mooney, W. D., & Fan, J.-C. (2006). Crustal structure of mainland China from deep seismic sounding data. *Tectonophysics*, 420(1-2), 239-252. Liu, Q.-Y., Zhang, L.-Y., Zhang, C., & He, L.-J. (2016). Lithospheric thermal structure of the North China Craton and its geodynamic implications. *Journal of Geodynamics*, 102, 139-150. Liu, Y.-S., Gao, S., Jin, S.-Y., Hu, S.-H., Sun, M., Zhao, Z.-B., & Feng, J.-L. (2001). Geochemistry of lower crustal xenoliths from Neogene Hannuoba basalt, North China craton: implications for petrogenesis and lower crustal composition. *Geochimica et Cosmochimica Acta*, 65(15), 2589-2604. Ma, Q., & Xu, Y.-G. (2021). Magmatic perspective on subduction of Paleo-Pacific plate and initiation of big mantle wedge in East Asia. *Earth-Science Reviews*, 213, 103473. Menzies, M. A., Fan, W., & Ming, Z. (1993). Palaeozoic and Cenozoic lithoprobes and the loss of > 120 km of Archaean lithosphere, Sino-Korean craton. *Geological Society, London, Special Publications*, 76(1), 71-81. Mooney, W. D. (2015). Crust and lithospheric structure - Global crustal structure. In Schubert G. (Eds.), *Treatise of Geophysics (Second Edition)*(pp. 339-390). Elsevier. Nishimoto, S., Ishikawa, M., Arima, M., Yoshida, T., & Nakajima, J. (2008). Simultaneous high P-T measurements of ultrasonic compressional and shear wave velocities in Ichino-megata mafic xenoliths: Their bearings on seismic velocity perturbations in lower crust of northeast Japan arc. *Journal of Geophysical Research: Solid Earth*, 113(B12212). Pirajno, F. (2007). Ancient to modern earth: The role of mantle plumes in the making of continental crust. In Kranendonk M. J. v., Smithies R. H. & Bennett V. C. (Eds.), *Developments in Precambrian Geology*(pp. 1037-1064). Ronov, A., & Yaroshevsky, A. (1967). Chemical structure of the Earth's crust. *Geokhimiya*, 11, 1285-1309. Ronov, A., & Yaroshevsky, A. (1976). A new model for the chemical structure of the Earth's crust. *Geokhimiya*, 12, 1761-1795. Rudnick, R., & Gao, S. (2003). Composition of the continental crust. In Holland H. D. & Turekian K. K. (Eds.), *Treatise on Geochemistry*(pp. 1-64). Oxford, Pergamon. Rudnick, R., & Gao, S. (2014). Composition of the continental crust. In Holland H. D. & Turekian K. K. (Eds.), *Treatise on Geochemistry (Second Edition)*(pp. 1-51). Oxford, Elsevier. Rudnick, R., & Presper, T. (1990). Geochemistry of intermediate/-to high-pressure granulites, *Granulites and crustal evolution*(pp. 523-550). Springer. Rudnick, R. L., & Fountain, D. M. (1995). Nature and composition of the continental crust: A lower crustal perspective. *Reviews of Geophysics*, 33(3), 267-309. Rudnick, R. L., & Taylor, S. R. (1987). The composition and petrogenesis of the lower crust: A xenolith study. *Journal of Geophysical Research: Solid Earth*, 92(B13), 13981-14005. Ruppel, C. (1995). Extensional processes in continental lithosphere. *Journal of Geophysical Research: Solid Earth*, 100(B12), 24187-

24215. Sammon, L. G., Gao, C., & McDonough, W. F. (2020). Lower crustal composition in the southwestern United States. *Journal of Geophysical Research: Solid Earth*, 125(3), e2019JB019011. Sammon, L. G., McDonough, W. F., & Mooney, W. D. (2022). Compositional attributes of the deep continental crust inferred from geochemical and geophysical data. *Journal of Geophysical Research: Solid Earth*, 127(8). Shaw, D., Cramer, J., Higgins, M., & Truscott, a. G. (1986). Composition of the Canadian Precambrian shield and the continental crust of the Earth. *Geological Society, London, Special Publications*, 24(1), 275-282. Shaw, D. M., Dickin, A. P., Li, H., McNutt, R. H., Schwarcz, H. P., & Truscott, M. G. (1994). Crustal geochemistry in the Wawa-Foley region, Ontario. *Canadian Journal of Earth Sciences*, 31(7), 1104-1121. Shaw, D. M., Reilly, G. A., Muysson, J. R., Pattenden, G. E., & Campbell, F. E. (1967). An estimate of the chemical composition of the Canadian precambrian shield. *Canadian Journal of Earth Sciences*, 4(5), 829-853. Shen, A. H., Bassett, W. A., & Chou, I. M. (1993). The alpha-beta quartz transition at high temperatures and pressures in a diamond-anvil cell by laser interferometry. *American Mineralogist*, 78(7), 694-698. Shinevar, W. J., Behn, M. D., & Hirth, G. (2015). Compositional dependence of lower crustal viscosity. *Geophysical Research Letters*, 42(20), 8333-8340. Shinevar, W. J., Behn, M. D., Hirth, G., & Jagoutz, O. (2018). Inferring crustal viscosity from seismic velocity: Application to the lower crust of Southern California. *Earth and Planetary Science Letters*, 494, 83-91. Smithson, S. B. (1978). Modeling continental crust: structural and chemical constraints. *Geophysical Research Letters*, 5(9), 749-752. Spencer, C. J., Roberts, N. M. W., & Santosh, M. (2017). Growth, destruction, and preservation of Earth's continental crust. *Earth-Science Reviews*, 172, 87-106. Sun, S. s., & McDonough, W. F. (1989). Chemical and isotopic systematics of oceanic basalts: implications for mantle composition and processes. *Geological Society, London, Special Publications*, 42(1), 313-345. Taylor, S. R. (1964). Abundance of chemical elements in the continental crust: A new table. *Geochimica et Cosmochimica Acta*, 28(8), 1273-1285. Taylor, S. R., & McLennan, S. M. (1985). The continental crust: its composition and evolution. In Hallam A. (Eds.), Blackwell scientific publication. Teng, J.-W., Zhang, Z.-J., Zhang, X.-K., Wang, C.-Y., Gao, R., Yang, B.-J., Qiao, Y.-H., & Deng, Y.-F. (2013). Investigation of the Moho discontinuity beneath the Chinese mainland using deep seismic sounding profiles. *Tectonophysics*, 609, 202-216. Thybo, H., & Artemieva, I. M. (2013). Moho and magmatic underplating in continental lithosphere. *Tectonophysics*, 609, 605-619. Wang, G.-C., Thybo, H., & Artemieva, I. M. (2021). No mafic layer in 80 km thick Tibetan crust. *Nature communications*, 12(1), 1-9. Weaver, B. L., & Tarney, J. (1984). Empirical approach to estimating the composition of the continental crust. *Nature*, 310(5978), 575-577. Wedepohl, K. H. (1995). The composition of the continental crust. *Geochimica et Cosmochimica Acta*, 59(7), 1217-1232. White, Powell, Holland, & Worley (2000). The effect of TiO<sub>2</sub> and Fe<sub>2</sub>O<sub>3</sub> on metapelitic assemblages at greenschist and amphibolite facies conditions: mineral equilibria calculations in the system K<sub>2</sub>O-FeO-MgO-Al<sub>2</sub>O<sub>3</sub>-SiO<sub>2</sub>-H<sub>2</sub>O-TiO<sub>2</sub>-Fe<sub>2</sub>O<sub>3</sub>. *Journal of Metamorphic Geology*, 18(5), 497-511. White, R. W., Powell, R., & Clarke, G. L. (2002).

The interpretation of reaction textures in Fe-rich metapelitic granulites of the Musgrave Block, central Australia: constraints from mineral equilibria calculations in the system  $K_2O-FeO-MgO-Al_2O_3-SiO_2-H_2O-TiO_2-Fe_2O_3$ . *Journal of Metamorphic Geology*, 20(1), 41-55. White, R. W., Powell, R., Holland, T. J. B., Johnson, T. E., & Green, E. C. R. (2014). New mineral activity-composition relations for thermodynamic calculations in metapelitic systems. *Journal of Metamorphic Geology*, 32(3), 261-286. White, W. M., & Klein, E. M. (2014). Composition of the oceanic crust. In Holland H. D. & Turekian K. K. (Eds.), *Treatise on Geochemistry (Second Edition)*(pp. 457-496). Oxford, Elsevier. Willbold, M., & Stracke, A. (2010). Formation of enriched mantle components by recycling of upper and lower continental crust. *Chemical Geology*, 276(3-4), 188-197. Wilson, J. T. (1968). Static or mobile earth: The current scientific revolution. *Proceedings of the American Philosophical Society* 112, 309-320. Wu, F.-Y., Yang, J.-H., Xu, Y.-G., Wilde, S. A., & Walker, R. J. (2018). Destruction of the North China Craton in the Mesozoic. *Annual Review of Earth and Planetary Sciences*, 47(1). Xia, B., Thybo, H., & Artemieva, I. M. (2017). Seismic crustal structure of the North China Craton and surrounding area: Synthesis and analysis. *Journal of Geophysical Research: Solid Earth*, 122(7), 5181-5207. Xia, Q.-K., Liu, J., Kovács, I., Hao, Y.-T., Li, P., Yang, X.-Z., Chen, H., & Sheng, Y.-M. (2019). Water in the upper mantle and deep crust of eastern China: concentration, distribution and implications. *National Science Review*, 6(1), 125-144. Xu, Y.-G. (2001). Thermo-tectonic destruction of the Archaean lithospheric keel beneath the Sino-Korean craton in China: evidence, timing and mechanism. *Physics and Chemistry of the Earth, Part A: Solid Earth and Geodesy*, 26(9-10), 747-757. You, Z.-D., & Chen, N.-S. (1995). The metamorphism of deeper crust in the Dabie mountains: as evidenced by the study of granulites near Huilanshan, Luotian. *Acta Petrologica Sinica*, 11(2), 137-147. Zertani, S., John, T., Tilmann, F., Motra, H. B., Keppler, R., Andersen, T. B., & Labrousse, L. (2019). Modification of the seismic properties of subducting continental crust by eclogitization and deformation processes. *Journal of Geophysical Research: Solid Earth*, 124(9), 9731-9754. Zhai, M.-G. (2011). Cratonization and the Ancient North China Continent: A summary and review. *Science China Earth Sciences*, 54(8), 1110-1120. Zhang, S.-H., Zhao, Y., Davis, G. A., Ye, H., & Wu, F. (2014). Temporal and spatial variations of Mesozoic magmatism and deformation in the North China Craton: Implications for lithospheric thinning and decratonization. *Earth-Science Reviews*, 131, 49-87. Zhang, Z.-J., Bai, Z.-M., Klempner, S. L., Tian, X.-B., Xu, T., Chen, Y., & Teng, J.-W. (2013). Crustal structure across northeastern Tibet from wide-angle seismic profiling: Constraints on the Caledonian Qilian orogeny and its reactivation. *Tectonophysics*, 606, 140-159. Zhang, Z.-J., Zhang, X., & Badal, J. (2008). Composition of the crust beneath southeastern China derived from an integrated geophysical data set. *Journal of Geophysical Research: Solid Earth*, 113(B04417). Zhang, Z.-M., Ding, H.-X., Palin, R. M., Dong, X., Tian, Z.-L., & Chen, Y.-F. (2020). The lower crust of the Gangdese magmatic arc, southern Tibet, implication for the growth of continental crust. *Gondwana Research*, 77, 136-146. Zhu, R.-X., & Xu, Y.-G. (2019). The subduction of the west Pacific

plate and the destruction of the North China Craton. *Science China Earth Sciences*, 62(9), 1340-1350. Zhu, R.-X., Yang, J.-H., & Wu, F.-Y. (2012). Timing of destruction of the North China Craton. *Lithos*, 149, 51-60.